

# The alignment of the second velocity moment tensor in galaxies

N. W. Evans,<sup>1</sup>★ J. L. Sanders,<sup>1</sup> A. A. Williams,<sup>1</sup> J. An,<sup>2</sup> D. Lynden-Bell<sup>1</sup>  
and W. Dehnen<sup>3</sup>

<sup>1</sup>*Institute of Astronomy, University of Cambridge, Madingley Road, Cambridge CB3 0HA, UK*

<sup>2</sup>*National Astronomical Observatories, Chinese Academy of Sciences, A20 Datun Road, Chaoyang District, Beijing 100012, PR China*

<sup>3</sup>*Department for Physics and Astronomy, University of Leicester, Leicester LE1 7RH, UK*

Accepted 2015 November 18. Received 2015 November 16; in original form 2015 September 2

## ABSTRACT

We show that provided the principal axes of the second velocity moment tensor of a stellar population are generally unequal and are oriented perpendicular to a set of orthogonal surfaces at each point, then those surfaces must be confocal quadric surfaces and the potential must be separable or Stäckel. This is true under the mild assumption that the even part of the distribution function (DF) is invariant under time reversal  $v_i \rightarrow -v_i$  of each velocity component. In particular, if the second velocity moment tensor is everywhere exactly aligned in spherical polar coordinates, then the potential must be of separable or Stäckel form (excepting degenerate cases where two or more of the semi-axes of ellipsoid are everywhere the same). The theorem also has restrictive consequences for alignment in cylindrical polar coordinates, which is used in the popular Jeans Anisotropic Models (JAM) of Cappellari. We analyse data on the radial velocities and proper motions of a sample of  $\sim 7300$  stars in the stellar halo of the Milky Way. We provide the distributions of the tilt angles or misalignments from both the spherical polar coordinate systems. We show that in this sample the misalignment is always small (usually within  $3^\circ$ ) for Galactocentric radii between  $\sim 6$  and  $\sim 11$  kpc. The velocity anisotropy is very radially biased ( $\beta \approx 0.7$ ), and almost invariant across the volume in our study. Finally, we construct a triaxial stellar halo in a triaxial NFW dark matter halo using a made-to-measure method. Despite the triaxiality of the potential, the velocity ellipsoid of the stellar halo is nearly spherically aligned within  $\sim 6^\circ$  for large regions of space, particularly outside the scale radius of the stellar halo. We conclude that the second velocity moment ellipsoid can be close to spherically aligned for a much wider class of potentials than the strong constraints that arise from exact alignment might suggest.

**Key words:** Galaxy: halo – galaxies: haloes – galaxies: kinematics and dynamics – dark matter.

## 1 INTRODUCTION

The Jeans equations relate the gravitational potential of a galaxy to the kinematic properties of the stars. This is an attractive way to infer the underlying mass, without the complexities of specifying a full phase space distribution function (DF). In this paper, we shall usually work with the second velocity moment tensor, which is just

$$\langle v_i v_j \rangle = \frac{1}{\rho} \int f v_i v_j d^3 v. \quad (1)$$

Here, the subscript indices denote one of the orthogonal coordinate directions, and the angled brackets represent averaging over the phase space DF  $f$ , whilst  $\rho$  is the density (see e.g. Binney & Tremaine 2008).

The second velocity moment tensor is sometimes separated into contributions from streaming motion and random motion by defining the velocity dispersion tensor

$$\sigma_{ij}^2 \equiv \langle (v_i - \langle v_i \rangle)(v_j - \langle v_j \rangle) \rangle. \quad (2)$$

In the absence of streaming motions, the second moment tensor and the velocity dispersion tensor are identical. The second moment tensor is a symmetric second-rank tensor and so may always be diagonalized. The principal axes of the tensor then form an ellipsoid, which we shall call the second moment ellipsoid. In the absence of streaming motions, this is just the velocity ellipsoid. This paper studies the alignment of the second moment ellipsoid and its implications for the underlying gravitational potential.

The Jeans equations are the first-order moments of the collisionless Boltzmann equation. They are three equations relating the six independent components of the second velocity moment tensor

★E-mail: [nwe@ast.cam.ac.uk](mailto:nwe@ast.cam.ac.uk)

$\langle v_i v_j \rangle$  to the density and the potential. Hence, the Jeans equations cannot uniquely determine the  $\langle v_i v_j \rangle$  and some closure condition must be adopted. A common choice is the alignment of the second moment ellipsoid in some coordinate system, which reduces the number of independent variables from six to three – namely, the semi-axes of the ellipsoid. For example, Cappellari (2008) provided an elegant way to solve the Jeans equations, assuming alignment in the cylindrical polar coordinate system  $(R, \phi, z)$ . These models – Jeans anisotropic models or JAM – have become widely used in analyses of integral field data on elliptical galaxies (see e.g. Cappellari et al. 2013), as well as studies of nuclear clusters (Hartmann et al. 2011) and lensing galaxies (van de Ven et al. 2010). Cylindrically aligned solutions with two of the semi-axes equal (i.e.  $\langle v_R^2 \rangle = \langle v_z^2 \rangle$ ) are generated by DFs depending on the two isolating integrals, energy  $E$  and angular momentum component  $L_z$  (Jeans 1919). When all three semi-axes are different, the validity of the JAM solutions remains unclear. In fact, Binney (2014) has already questioned whether construction of numerical DFs for models with such properties is possible.

Alignment in the spherical polar coordinate system  $(r, \theta, \phi)$  is also often used in the Jeans equations. If two of the semi-axes are equal (i.e.  $\langle v_\theta^2 \rangle = \langle v_\phi^2 \rangle$ ), then the spherical aligned solutions can be generated by DFs depending on the two integrals, energy  $E$  and square of the angular momentum  $L^2$ . Assuming a spherical density and potential, this ansatz is very popular as the Jeans equations then reduce to a single equation for the radial velocity dispersion  $\langle v_r^2 \rangle$  together with an anisotropy parameter  $\beta(r)$

$$\beta(r) = 1 - \frac{\langle v_\theta^2 \rangle}{\langle v_r^2 \rangle}. \quad (3)$$

Given a choice for  $\beta(r)$ , the only non-trivial Jeans equations can be straightforwardly solved using an integrating factor (see e.g. van der Marel 1994; An & Evans 2011; Agnello, Evans & Romanowsky 2014). Algorithms for solution of the Jeans equations using spherical alignment but flattened densities and potentials have also been developed (see e.g. Bacon, Simien & Monnet 1983; Bacon 1985; Evans, Hafner & de Zeeuw 1997; Evans et al. 2015). These can in general have three different principal axes  $\langle v_r^2 \rangle$ ,  $\langle v_\theta^2 \rangle$  and  $\langle v_\phi^2 \rangle$  and so the second moment ellipsoid is triaxial, but whether they can be realized by physical (non-negative) DFs remains unclear.

Alignment in spheroidal coordinates  $(\lambda, \mu, \phi)$  has also been studied. This coordinate system is described in, for example, Morse & Feshbach (1953) or Binney & Tremaine (2008). Within the foci of the coordinate system, spheroidal alignment approaches cylindrical, whilst at large radii, it tends to spherical. Spheroidal alignment can therefore be viewed as interpolating between these two more familiar cases. It has long been known that if the gravitational potential is of Stäckel or separable form, then the second moment ellipsoid is aligned in spheroidal coordinates (see e.g. Eddington 1915; Lynden-Bell 1962; Evans & Lynden-Bell 1989). However, the assumption that the ellipsoid is aligned in spheroidal coordinates can be made without a separable potential (Arnold 1995). In fact, this makes good sense, as models of axisymmetric galaxies using numerical constructed DFs do suggest the alignment may be close to spheroidal (e.g. Dehnen & Gerhard 1993; Binney 2014). Intuitively, for systems like the stellar halo of the Milky Way, the potential in the inner parts is controlled by the flattened disc and bulge, in the outer parts by the rounder dark matter halo, and so again an alignment in spheroidal coordinates does seem very natural.

Spheroidal coordinates are the axisymmetric limit of ellipsoidal coordinates  $(\lambda, \mu, \nu)$ . For triaxial Stäckel models, Eddington (1915) already knew that the second velocity moment ellipsoid is aligned in

ellipsoidal coordinates. The triaxial Jeans equations for such Stäckel systems have been studied sporadically (Lynden-Bell 1960; Evans & Lynden-Bell 1989; van de Ven et al. 2003). Given the density and potential, the Jeans equations are now three coupled first-order partial differential equations for three unknowns, namely  $\langle v_\lambda^2 \rangle$ ,  $\langle v_\mu^2 \rangle$  and  $\langle v_\nu^2 \rangle$ . Both the prescription of appropriate boundary conditions and the solution of the equations is challenging. Only very few general triaxial DFs have ever been numerically constructed. The few such models available do show approximate alignment in ellipsoidal coordinates (e.g. Sanders & Evans 2015).

Our intention in this paper is to examine what may be legitimately deduced about the underlying gravitational potential from the alignment of the second velocity moment ellipsoid. This is motivated by arguments of Smith, Evans & An (2009b) who claim that: “if a steady state stellar population has a triaxial velocity dispersion tensor whose eigenvectors are everywhere aligned in spherical polar coordinates, then the underlying gravitational potential must be spherically symmetric”. This theorem will be examined, slightly corrected, and then extended below.

This argument was queried by Binney & McMillan (2011), who created a torus-based model of the Galaxy that, at locations above the plane of the Milky Way, possessed a spherically aligned velocity dispersion tensor, even though the potential was highly flattened. Although Binney & McMillan (2011) did not provide an explicit counter-example to the theorem of Smith et al. (2009b), they did question whether in general the potential does control the tilt. In their numerically constructed example, they argued that the tilt of the second velocity moment ellipsoid is controlled at least as much by the weightings of orbits, and hence the DF, as compared to the potential. In this respect, Binney & McMillan (2011) conjectured that insights from separable or Stäckel models may not tell the whole story. One of the aims of this paper is to resolve the tension between these two viewpoints.

The paper is organized as follows. Section 2 studies the one spheroidal system for which there is hard data on the alignment – namely, the stellar halo of the Milky Way galaxy. For elliptical galaxies, evidence on the alignment is necessarily much more indirect, as only the line-of-sight velocity distribution can be measured. We confirm, and sharpen, the results of Smith et al. (2009b) and Bond et al. (2010) that the velocity ellipsoid of stars in the Milky Way stellar halo is close to spherical or spheroidal alignment. Section 3 is theoretical and examines the case of exact spherical alignment. We prove under quite general conditions that the gravitational potential must be of separable or Stäckel form in spheroidal polars. This is an elaboration of the original theorem of Smith et al. (2009b). The only exceptions are simpler cases in which the second velocity moment ellipsoid has either two axes the same and so is a spheroid, or three axes the same and so is a sphere. Section 4 discusses cylindrical and spheroidal alignment, and demonstrates, for the first time, that the assumption of alignment of the (assumed triaxial) second velocity moment tensor implies separability of the Hamilton–Jacobi equation in these coordinates. The converse result – that the separable or Stäckel potentials generate galaxy models in which the second velocity moment tensor is aligned along the separable coordinate system – has been known for some time and is implicit in Eddington’s early work (Eddington 1915; Lynden-Bell 1962; Evans 2011). Lastly, Section 5 builds models of stellar haloes in which the second velocity moment tensor is close to, but not exactly, spherically aligned and tests whether results remain valid in this approximate regime. We show that it is possible to build haloes in flattened potentials in which the velocity ellipsoid is close to spherical alignment over substantial portions of

configuration space, though not everywhere. However, the more the potential is flattened, the greater is the magnitude and extent of the misalignment.

## 2 THE STELLAR HALO OF THE MILKY WAY

### 2.1 Background

The study of the kinematics of stars in the Milky Way halo has been revolutionized by high-quality data derived from the Sloan Digital Sky Survey (SDSS). Line-of-sight velocities are extracted from SDSS spectroscopy. Proper motions are derived from either multi-epoch SDSS photometry in Stripe 82 (Bramich et al. 2008) or from matches to archival Schmidt photographic-plate based catalogues (Munn et al. 2004). So, all three components of velocities are now available for thousands of halo stars, together with positions and photometric parallaxes.

Smith et al. (2009a,b) constructed a sample of halo subdwarfs using a reduced proper motion diagram, utilizing the light-motion catalogue for Stripe 82 (Bramich et al. 2008). They extracted a clean sample of 1782 halo stars, lying at Galactocentric cylindrical polar radii between 7 and 10 kpc, and at depths of 4.5 kpc or less below the Galactic plane. They found the first velocity moments to be consistent with zero to within the statistical error – see table 2 of Smith et al. (2009a). So, the second velocity moments ( $\langle v_r^2 \rangle$ ,  $\langle v_\theta^2 \rangle$ ,  $\langle v_\phi^2 \rangle$ ) are equivalent to the velocity dispersions ( $\sigma_r^2$ ,  $\sigma_\theta^2$ ,  $\sigma_\phi^2$ ), which we use henceforth in this section. They also found that the velocity ellipsoid of the halo stars is aligned with the spherical polar coordinate system, with the long axis pointing towards the Galactic Centre. The halo stars are strongly radially anisotropic. The semiaxes of the velocity ellipsoid are  $(\sigma_r, \sigma_\theta, \sigma_\phi) = (143 \pm 2, 77 \pm 2, 82 \pm 2)$   $\text{kms}^{-1}$ , which corresponds to an anisotropy parameter

$$\beta = 1 - \frac{\sigma_\theta^2 + \sigma_\phi^2}{2\sigma_r^2} \quad (4)$$

of 0.69. They also noted a tentative asymmetry in the  $v_\phi$  distribution, but found the  $v_r$  and  $v_\theta$  distributions symmetric.

This conclusion was reinforced by the larger sample of Bond et al. (2010). Here, halo stars are extracted from the SDSS data by combined colour and metallicity cuts (specifically  $0.2 < g - r < 0.4$  and  $[\text{Fe}/\text{H}] < -1.1$ ). Requiring the stars possess SDSS spectra for radial velocities and POSS astrometry for proper motions yields a large sample of  $\sim 7400$  halo stars, with an estimated contamination of  $\sim 6$  per cent. Bond et al. (2010) found that the shape of the velocity ellipsoid is invariant in spherical coordinates within the volume probed by SDSS and aligned in spherical polar coordinates (their figs 12 and 13). They found no statistically significant tilt from spherical alignment, with deviations modest and ranging between  $1^\circ$  to  $5^\circ$ . Note that this sample extends over Galactocentric cylindrical polar radii  $6 \lesssim R \lesssim 11$  kpc and height above the Galactic plane  $3 \lesssim |z| \lesssim 5$  kpc, and so is much more extensive than earlier work. None the less, the semiaxes of the velocity ellipsoid are  $(\sigma_r, \sigma_\theta, \sigma_\phi) = (141 \pm 5, 75 \pm 5, 85 \pm 5)$   $\text{kms}^{-1}$ , in very good agreement with Smith et al. (2009a). Bond et al's error bars also include systematic effects such as errors in the photometric parallaxes, whereas Smith et al's do not.

Very recently, King et al. (2015) have examined a still larger sample of halo stars with Galactocentric radii between 6 and 30 kpc. This contains blue horizontal branch (BHB) and halo F stars extracted from SDSS, as well as a sample of still more distant F stars obtained from Hectospec on the MMT. Although only line of sight velocities are available, this still can yield constraints on the alignment,

as there are different contributions from both radial and tangential velocities in different directions on the sky. King et al. (2015) find the alignment of the velocity ellipsoid of their halo sample to be close to spherical, albeit to within quite large uncertainties.

### 2.2 Alignment and symmetries

Here, we will re-analyse the data of Bond et al. (2010). We first discuss how the errors on the observable quantities propagate through to the alignment. The errors on the radial velocities are computed by the SDSS pipeline, to which should be added a systematic error of between  $2 \text{ km s}^{-1}$  (optimistic) and  $6 \text{ km s}^{-1}$  (pessimistic). The proper-motion errors are discussed in Bond et al. (2010), who suggest using a fixed value of  $0.6 \text{ mas yr}^{-1}$ . We assume that there is zero covariance between the two proper-motion components.

The SDSS pipeline provides photometric errors, which can be used to compute random errors in absolute magnitude (assuming that the interband covariances are negligible). Polynomial relations for the absolute magnitude of F and G stars as a function of  $g$ ,  $r$ ,  $i$  and metallicity  $[\text{Fe}/\text{H}]$  are given in Ivezić et al. (2008). We then use Monte Carlo methods to gain an estimate of the random error in the absolute magnitude, given the errors in  $g$ ,  $r$ ,  $i$  and  $[\text{Fe}/\text{H}]$ , and add 0.1 mag in quadrature to account for systematics. Given the estimates of error in the absolute magnitude (with systematics included), we use Monte Carlo methods to estimate the error on the distances of each star in the sample.

To extract the halo sample, we apply the cuts  $0.2 < g - r < 0.6$  and  $-3.0 < [\text{Fe}/\text{H}] < -1.1$  to the data. We then restrict ourselves to stars that are found in the volume  $6 < R/\text{kpc} < 11$  and  $3 < |z|/\text{kpc} < 5$ . This gives us a final sample of 7418 stars (5006 above the plane and 2412 below).

Fig. 1 depicts the velocity distributions of our samples. Just through visual inspection, it is clear that the velocity ellipsoid cannot be aligned with cylindrical coordinates, as the  $(v_R, v_z)$  distribution has a noticeable tilt. The green dashed lines in the plot are at an angle  $\arctan(z/R)$ , the direction that the long axis of the distribution should point if spherical alignment is satisfied. By eye, the tilt of the velocity distributions seems to be in good agreement with spherical alignment. This motivates a quantitative analysis of the data.

### 2.3 Inference on properties of the velocity distributions

Given three orthogonal velocity components,  $(v_i, v_j, v_k)$ , the tilt angle,  $\alpha_{ij}$ , is the angle between the  $i$ -axis and the major axis of the ellipse formed by projecting the three-dimensional velocity ellipsoid on to the  $ij$ -plane (see e.g. Binney & Merrifield 1998 or appendix A of Smith et al. 2009b).

$$\tan(2\alpha_{ij}) = \frac{2\sigma_{ij}^2}{\sigma_{ii}^2 - \sigma_{jj}^2}. \quad (5)$$

Our aim is to diagnose the degree of misalignment in the data. We do so by using a probabilistic method and a simple model of the velocity distributions in some coordinate system. We split the data into six annular bins in  $(R, z, \phi)$ . Each bin spans the whole range of  $\phi$ . There are three bins above the plane and three below it – in all cases, the vertical range is  $3 < |z|/\text{kpc} < 5$ . We then split the data in to three equally spaced radial bins within the range  $6 < R/\text{kpc} < 11$ . Within each bin, we make the simplifying assumption that the density distribution is uniform, so that

$$p(R, z, \phi) = U(R, z, \phi). \quad (6)$$

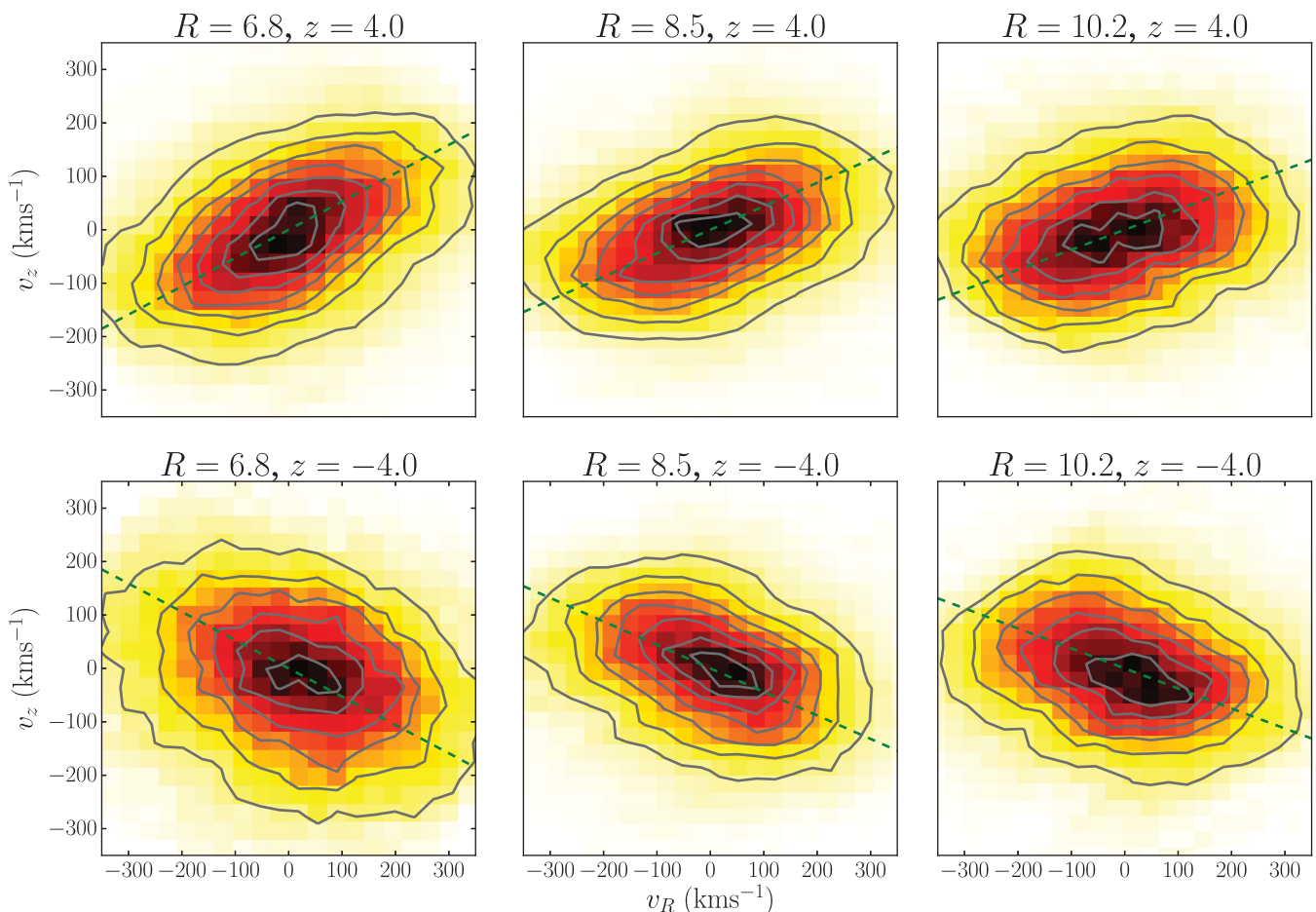


**Figure 1.** Velocity distributions of our halo sample in  $(v_R, v_z)$  space in six spatial bins. The position of each bin centroid  $(R, z)$  is written in kpc above the plot of the velocity distributions in that bin. The green dashed lines are at an angle  $\arctan(z/R)$  where  $(R, z)$  is the position of the bin centroid. The long axis of the  $(v_R, v_z)$  distribution should coincide with this line if the velocity ellipsoid is spherically aligned.

We then model the velocity distribution in each bin as a three-dimensional normal distribution in the three relevant (orthogonal) velocity components  $(v_1, v_2, v_3)$ . Here, we focus on the spherical and prolate spheroidal cases. The normal distribution has mean  $\boldsymbol{\mu} = \langle \mathbf{v} \rangle$  and covariance matrix

$$\boldsymbol{\Sigma} = \begin{bmatrix} \sigma_1^2 & \frac{1}{2}(\sigma_1^2 - \sigma_2^2) \tan 2\alpha_{12} & \frac{1}{2}(\sigma_1^2 - \sigma_3^2) \tan 2\alpha_{13} \\ \cdot & \sigma_2^2 & \frac{1}{2}(\sigma_2^2 - \sigma_3^2) \tan 2\alpha_{23} \\ \cdot & \cdot & \sigma_3^2 \end{bmatrix}, \quad (7)$$

where  $\sigma_i$  are the velocity dispersions and  $\alpha_{ij}$  are the misalignment angles as previously defined, and the matrix is by construction symmetric. The parameters of the model (per bin) are then  $\mathcal{P} = (\langle \mathbf{v} \rangle, \boldsymbol{\sigma}, \boldsymbol{\alpha})$ . We then compute the likelihood for individual stars within a given bin as

$$p(\mathbf{L}|\mathcal{P}) = \int d\mathbf{L}' p(\mathbf{L}|\mathbf{L}', \mathbf{C}) p(\mathbf{L}'|\mathcal{P}), \quad (8)$$

where  $\mathbf{L} = (s, l, b, v_{\text{LOS}}, \boldsymbol{\mu})$ . We assume Gaussian errors in the data, with some covariance matrix  $\mathbf{C}$  that is diagonal – which is tantamount to assuming that errors on the observed quantities are not correlated. Thus,  $p(\mathbf{L}|\mathbf{L}', \mathbf{C})$  is a six-dimensional normal distribution with a diagonal covariance matrix, although in practise we assume that the measurements of  $l$  and  $b$  are error-free. Our model is expressed in the coordinate system given by  $\mathbf{w} = (R, z, \phi, v_i, v_j, v_k)$

$$p(\mathbf{w}|\mathcal{P}) = \mathcal{U}(R, z, \phi) \mathcal{N}(\mathbf{v}, \langle \mathbf{v} \rangle, \boldsymbol{\Sigma}), \quad (9)$$

where  $\mathcal{N}$  is the normal distribution. Equation (9) is related to the distribution  $p(\mathbf{L}'|\mathcal{P})$  by the Jacobian factor

$$p(\mathbf{L}'|\mathcal{P}) = p(\mathbf{w}|\mathcal{P}) \left| \frac{\partial \mathbf{w}}{\partial \mathbf{L}'} \right|, \\ = p(\mathbf{w}|\mathcal{P}) \frac{s'^4 \cos b'}{R(s', l', b')}, \quad (10)$$

where  $R(s', l', b')$  is the cylindrical  $R$  coordinate expressed in terms of the line-of-sight distance and galactic longitude and latitude. Thus, the final expression for the likelihood of an individual star in a given bin is

$$p(\mathbf{L}|\mathcal{P}) \\ = \int d\mathbf{L}' p(\mathbf{L}|\mathbf{L}', \mathbf{C}) \mathcal{U}(R', z', \phi') \mathcal{N}(\mathbf{v}', \boldsymbol{\mu}, \boldsymbol{\Sigma}) \frac{s'^4 \cos b'}{R(s', l', b')}. \quad (11)$$

In order to approximate this likelihood, we draw  $N$  samples from the error ellipsoids of each star [i.e. we sample the distribution  $p(\mathbf{L}|\mathbf{L}', \mathbf{C})$ ] and evaluate the likelihood via the Monte-Carlo sum

$$p(\mathbf{L}|\mathcal{P}) \simeq \frac{1}{N} \sum_{i=0}^N \mathcal{U}(R'_i, z'_i, \phi'_i) \mathcal{N}(\mathbf{v}'_i, \boldsymbol{\mu}, \boldsymbol{\Sigma}) \frac{s'^4 \cos b'_i}{R(s'_i, l'_i, b'_i)}. \quad (12)$$

This is done for  $N = 100$  per star and the total likelihood is the product of equation (12) for every star in the bin. The log-likelihood is

**Table 1.** At each location ( $R, z$ ), the inferred values and  $1\sigma$  confidence intervals for each of the model parameters.

$(R, z)$ (kpc)	$\langle v_r \rangle$ ( $\text{km s}^{-1}$ )	$\langle v_\theta \rangle$ ( $\text{km s}^{-1}$ )	$\langle v_\phi \rangle$ ( $\text{km s}^{-1}$ )	$\sigma_r$ ( $\text{km s}^{-1}$ )	$\sigma_\theta$ ( $\text{km s}^{-1}$ )	$\sigma_\phi$ ( $\text{km s}^{-1}$ )	$\alpha_{r\theta}$ ( $^\circ$ )	$\alpha_{r\phi}$ ( $^\circ$ )	$\alpha_{\theta\phi}$ ( $^\circ$ )
(6.85,4.00)	$-4.3 \pm 4.2$	$-4.7 \pm 2.3$	$-8.6 \pm 2.9$	$161.2 \pm 3.1$	$88.7 \pm 1.8$	$106.8 \pm 2.3$	$-0.06 \pm 1.3$	$4.9 \pm 2.0$	$5.6 \pm 4.3$
(8.50,4.00)	$-2.2 \pm 3.7$	$-5.4 \pm 2.0$	$-8.9 \pm 2.4$	$150.8 \pm 2.7$	$76.1 \pm 1.6$	$89.7 \pm 2.0$	$-1.3 \pm 1.1$	$1.0 \pm 1.5$	$-0.2 \pm 5.3$
(10.15,4.00)	$-10.2 \pm 4.5$	$-2.6 \pm 2.9$	$-0.1 \pm 2.7$	$161.6 \pm 3.4$	$94.2 \pm 2.1$	$80.3 \pm 2.3$	$11.4 \pm 1.3$	$1.3 \pm 1.3$	$14.5 \pm 5.2$
(6.85,-4.00)	$10.5 \pm 8.8$	$5.5 \pm 5.9$	$3.3 \pm 6.5$	$149.3 \pm 7.1$	$73.3 \pm 4.8$	$103.2 \pm 5.2$	$2.5 \pm 3.0$	$-12.7 \pm 4.9$	$7.8 \pm 6.4$
(8.50,-4.00)	$-9.7 \pm 5.4$	$-4.6 \pm 3.1$	$-7.0 \pm 3.6$	$140.3 \pm 4.3$	$74.6 \pm 2.6$	$86.4 \pm 2.8$	$2.6 \pm 1.8$	$-0.3 \pm 2.3$	$3.4 \pm 8.0$
(10.15,-4.00)	$-5.0 \pm 4.5$	$-2.6 \pm 2.6$	$0.4 \pm 3.2$	$143.1 \pm 3.4$	$69.0 \pm 2.2$	$76.4 \pm 3.0$	$5.5 \pm 1.5$	$2.0 \pm 1.8$	$-4.8 \pm 12.8$

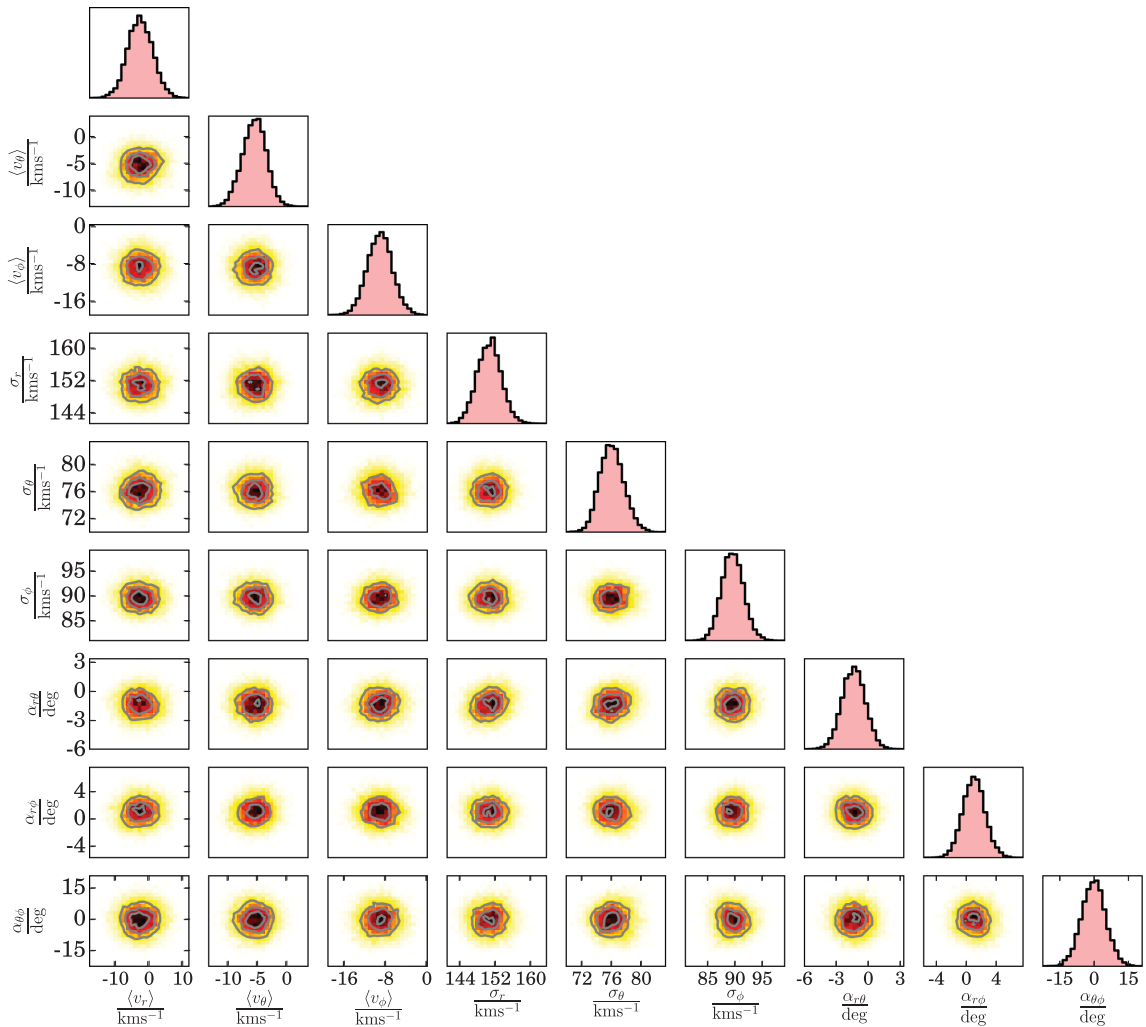
explored using the EMCEE ensemble sampler (Foreman-Mackey et al. 2013), implemented in PYTHON. In the end, we infer nine parameters for each of our six spatial bins (three mean velocities, three velocity dispersions and three misalignment angles). Our priors are uninformative, so that  $-45^\circ < \alpha_{ij} < 45^\circ$  and  $\sigma_i > 0$ .

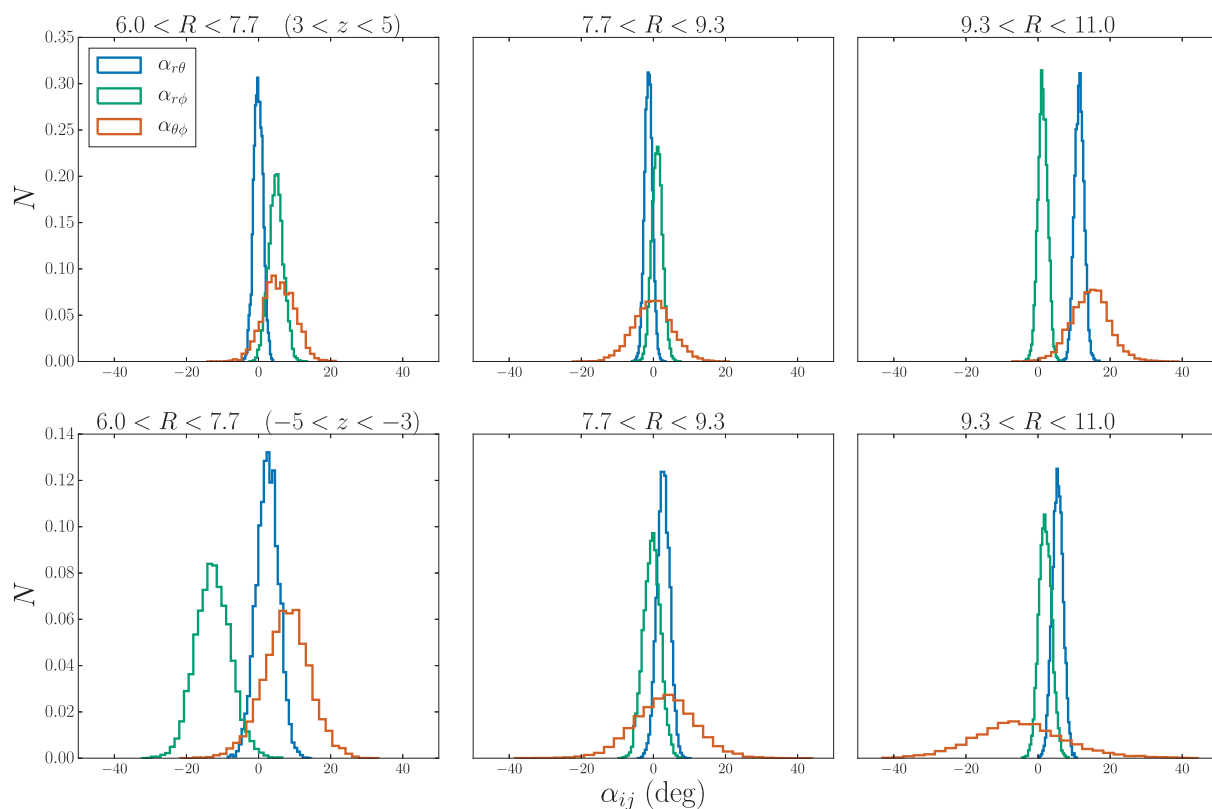
#### 2.4 Analysis in spherical coordinates

Table 1 gives the inferred values of the model parameters in each of our bins, as well as the  $1\sigma$  confidence intervals. In general, we

detect no strong correlations between any of the parameters – as an example, Fig. 2 shows the one- and two-dimensional projections of the posterior probability distribution in one of our bins.

We find that the misalignment angles are small, and that the velocity dispersions obey  $\sigma_r > \sigma_\phi > \sigma_\theta$  – consistent with a radially biased, flattened stellar halo. Fig. 3 gives the one-dimensional marginalized distributions on the misalignment angles in each of our bins, and Fig. 4 is the same but for the anisotropy parameter. The overall picture is of an extremely radially biased population, with  $\beta \sim 0.7$  almost invariant over the whole volume that we probe,

**Figure 2.** Inference on the parameters of the model described in Section 2.3 in the bin  $7.7 < R/\text{kpc} < 9.3$ ,  $3 < z/\text{kpc} < 5$ . We can see that there is no noticeable covariance between any of the model parameters, and that the tilt angles are all consistent with zero at (at least) the  $2\sigma$  level.



**Figure 3.** The marginalized posterior distributions on the misalignment angles in each bin. In most of the bins, the three angles are consistent with zero at the  $2\sigma$  level or better. The biggest discrepancy is in  $\alpha_{r\theta}$  in the above-plane bin spanning  $9.3 < R/\text{kpc} < 11.0$  (top-right panel). The angle with the largest uncertainty is always  $\alpha_{\theta\phi}$ , since  $\sigma_\theta$  and  $\sigma_\phi$  are the most similar of the three velocity dispersions.

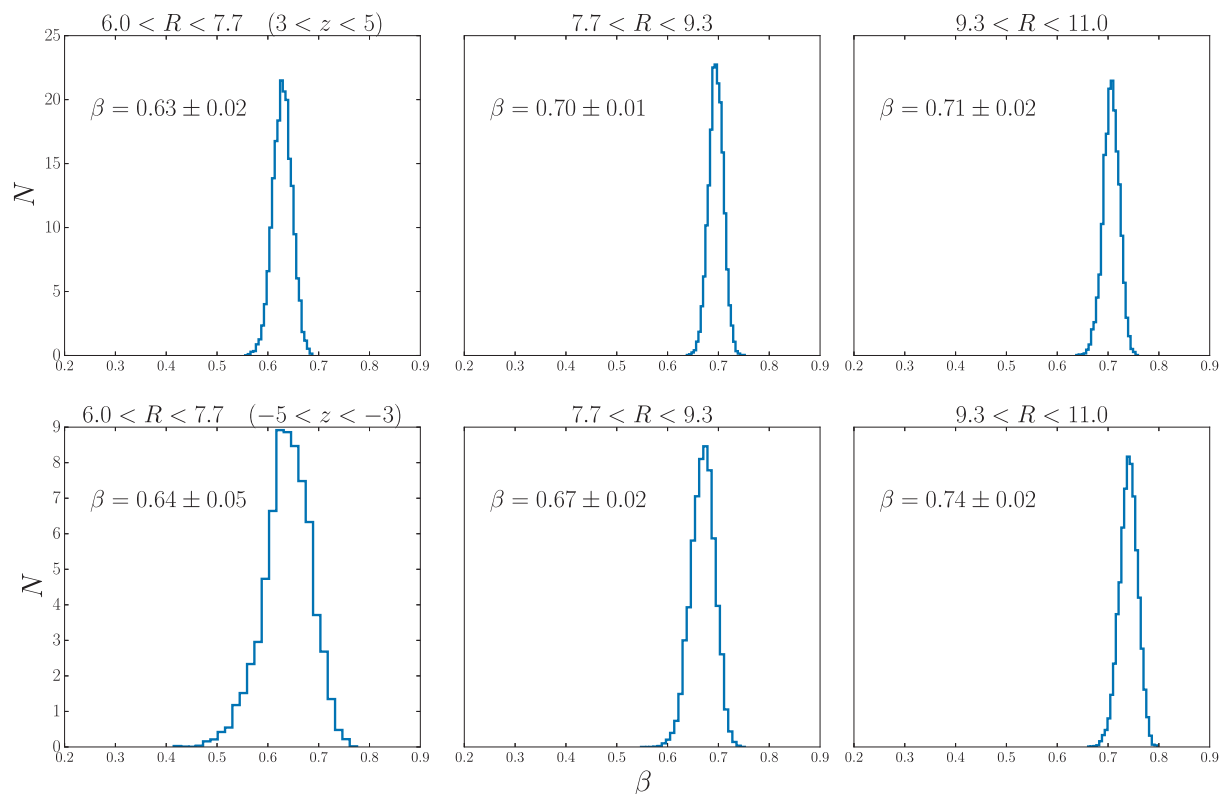


**Figure 4.** The distributions of the spherical anisotropy parameter calculated using the samples from our MCMC chains. The velocity anisotropy is very radially biased, and almost invariant across the volume in our study.

and velocity distributions that are close to spherically aligned – consistent with the findings of Bond et al. (2010) and Smith et al. (2009b,a). The inferred misalignment angles are usually  $\sim 3^\circ$  with uncertainties of a similar size, although there are a few cases where the misalignment is much larger. The most discrepant case is the bin with edges  $9.3 < R/\text{kpc} < 11.0$  and  $3 < z/\text{kpc} < 5$ , where  $\alpha_{r\theta} = 11.4^\circ \pm 1.3^\circ$ . Curiously, this bin is also the only of the six where  $\sigma_\theta > \sigma_\phi$ , which is perhaps suggestive that the contamination from either substructure or the thick disc is more significant in this bin.

We infer non-zero first-order moments in each of the velocity components. In the following sections, we shall see that the assumption of symmetry about  $\mathbf{v} = 0$  is necessary to relate the orientation of the velocity ellipsoids to properties of the matter distribution. Although it is the case that the first moments are often discrepant with zero at the  $1\sigma$  (or sometimes  $2\sigma$ ) level through inspection of the Monte-Carlo samples of posterior distributions, we do not believe that the results are truly significant. The first-order moments will be the most severely affected of our parameters by incorrect assumptions about the circular velocity at the solar position, as well as the velocity of the sun with respect to the LSR. In all of our analysis, we used the same values for these velocities as in Bond et al. (2010), and so uncertainties on them are not reflected in our posterior distributions. Given the fact that the first moments we infer are always  $\sim 10 \text{ km s}^{-1}$  or smaller, it is highly plausible that incorporating uncertainty on the circular speed and solar motion could account for these discrepancies from zero.

## 2.5 Spheroidal coordinates

Another coordinate system of interest is the prolate spheroidal system  $(\lambda, \mu, \phi)$ , often used in modelling oblate mass models (see e.g. de Zeeuw 1985; Dehnen & Gerhard 1993). These coordinates (which are discussed in greater detail in Section 4.2) are related to cylindrical polars via the set of equations

$$R = a \sinh \lambda \sin \mu,$$

$$z = a \cosh \lambda \cos \mu,$$

$$\phi = \phi. \quad (13)$$

Surfaces of constant  $\mu$  are hyperbolic sheets, whereas surfaces of constant  $\lambda$  are prolate ellipsoids. The quantity  $a$  is called the *focal distance*. At large distances from the origin, these surfaces begin to coincide with spherical polar coordinates ( $\lambda \sim r$  and  $\mu \sim \theta$ ), whereas at small distances the coordinate surfaces align with cylindrical polars ( $\lambda \sim R$  and  $\mu \sim z$ ). In order to compute properties of the velocity distributions, we must also express the velocities in this coordinate system. These are related to the cylindrical velocities via

$$v_\lambda = \frac{v_R \cosh \lambda \sin \mu + v_z \sinh \lambda \cos \mu}{\sinh^2 \lambda + \sin^2 \mu},$$

$$v_\mu = \frac{v_R \sinh \lambda \cos \mu - v_z \cosh \lambda \sin \mu}{\sinh^2 \lambda + \sin^2 \mu},$$

$$v_\phi = v_\phi. \quad (14)$$

Since there is a free parameter associated with this coordinate system,  $a$ , there are many possible different orientations of the velocity ellipsoids. In order to decide upon a value of  $a$  that gives the smallest misalignment angles in the distribution of  $(v_\lambda, v_\mu, v_\phi)$ , we employ a method identical to that described above, save for three differences.

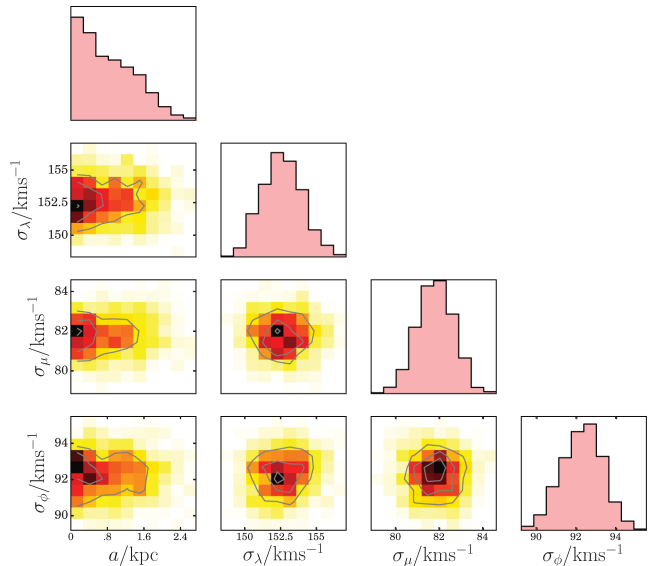


**Figure 5.** Inference on the best-fit spheroidal focal distance  $a$  and the velocity dispersions of the data. One can see that small foci are favoured, so that the spheroidal coordinate system essentially coincides with spherical polar coordinates.

We do not bin the data in this case, but instead simply model the velocity distribution as invariant across the entire volume. We assume that this distribution has zero mean ( $\boldsymbol{\mu} = \mathbf{0}$ ). We also alter the covariance matrix  $\boldsymbol{\Sigma}$  so that it now reads

$$\boldsymbol{\Sigma} = \begin{bmatrix} \sigma_\lambda^2 & 0 & 0 \\ \cdot & \sigma_\mu^2 & 0 \\ \cdot & \cdot & \sigma_\phi^2 \end{bmatrix}. \quad (15)$$

This is done because we are aiming for a value of  $a$  that minimizes misalignment, so our model is of a velocity distribution that has  $\boldsymbol{\alpha} = \mathbf{0}$  – this assumption provides the constraint on  $a$ . In this case, then, the model parameters are  $\mathcal{P} = (a, \sigma_\lambda, \sigma_\mu, \sigma_\phi)$ . If we were to bin the data, we would infer four parameters per bin, leading to a total of 24 parameters. By not binning the data, we reduce our parameter space to four dimensions, which takes significantly less computational time to sample. Despite our rather crude assumption that the velocity distribution is invariant in the volume we are studying, we expect this analysis to give a decent estimate of the focal distance that reduces misalignment. Again, we use EMCEE to do the sampling, with uninformative priors that simply ensure that all four of the model parameters are greater than zero.

Fig. 5 depicts the posterior probability distributions on the four parameters of the model. In particular, it is clear that the data favours coordinate systems that have a small focal distance – we infer  $a = 0_{-0}^{+0.8}$  kpc. In this limit, the prolate spheroidal coordinates coincide with spherical polars. The data, then, suggest that the extra degree of freedom provided by the prolate spheroidal coordinates does not produce better alignment of the velocity ellipsoid.

## 3 SPHERICAL ALIGNMENT

Motivated by our analysis of the stellar halo, let us assume that the second velocity moment ellipsoid is aligned with the spherical polar coordinate system. This means that all the cross terms  $\langle v_r v_\theta \rangle = \langle v_r v_\phi \rangle = \langle v_\theta v_\phi \rangle$  vanish. The DF depends on phase space coordinates and so may have the completely general form

$F(\mathbf{v}, \mathbf{x}) = F(v_r, v_\theta, v_\phi, r, \theta, \phi)$ . However, the DF is an integral of motion by Jeans Theorem, and so the Poisson bracket  $\{F(\mathbf{v}, \mathbf{x}), H\}$  must vanish. Under time reversal, integrals of motion remain integrals of motion, so the Poisson bracket  $\{F(-\mathbf{v}, \mathbf{x}), H\}$  must also vanish. Therefore, we can always construct the even function  $F_e = \frac{1}{2}[F(\mathbf{v}, \mathbf{x}) + F(-\mathbf{v}, \mathbf{x})]$ , which must depend on even powers of the velocities. This is of course just the even part of the DF.

The even part of the DF may contain terms like  $v_r^l v_\theta^m v_\phi^n$  provided  $l + m + n$  is itself even. However, the cross-terms  $\langle v_r v_\theta \rangle = \langle v_r v_\phi \rangle = \langle v_\theta v_\phi \rangle$  must all vanish at every position. On the grounds of naturalness, we expect that the DF must be of form  $F_e = F_e(v_r^2, v_\theta^2, v_\phi^2, r, \theta, \phi)$  and so it must depend only on even powers of the velocity components in the aligned coordinate system. This is a key step in the proof, though the condition can be recast in terms of the fourth velocity moments, albeit with some effort (An & Evans 2016). However, here we can appeal directly to the data – we have shown in the preceding section that the mean motions of velocity distributions of the stellar halo are consistent with zero in almost every bin. The velocity distributions are symmetric to a good approximation under the transformations  $v_r \rightarrow -v_r$  or  $v_\theta \rightarrow -v_\theta$  or  $v_\phi \rightarrow -v_\phi$  (see e.g. Fig. 1). In other words, without changing the underlying potential, we can always construct the even part of the DF, which must depend on even powers only of the individual velocity components. Smith et al. (2009b) reached the same conclusion that the DF may be chosen to depend only on even powers, but their line of reasoning was incorrect.

Introducing canonically conjugate momenta  $p_r = v_r$ ,  $p_\theta = r v_\theta$  and  $p_\phi = r \sin \theta v_\phi$  (Landau & Lifshitz 1976), then the Hamiltonian is

$$H = \frac{1}{2} \left( p_r^2 + \frac{p_\theta^2}{r^2} + \frac{p_\phi^2}{r^2 \sin^2 \theta} \right) - \psi(r, \theta, \phi), \quad (16)$$

where  $\psi$  is the gravitational potential. Without loss of generality, the DF can now be recast as  $F_e(H, p_\theta^2, p_\phi^2, r, \theta, \phi)$  by using the Hamiltonian to eliminate  $p_r^2$ . The Poisson bracket  $\{F_e, H\}$  must vanish. The  $H$  in the DF may be treated as a constant when evaluating the derivatives in the Poisson bracket, yielding

$$p_r \frac{\partial F_e}{\partial r} + \frac{p_\theta}{r^2} \frac{\partial F_e}{\partial \theta} + \frac{p_\phi}{r^2 \sin^2 \theta} \frac{\partial F_e}{\partial \phi} + \left( \frac{p_\phi^2 \cos \theta}{r^2 \sin^3 \theta} + \frac{\partial \psi}{\partial \theta} \right) \frac{\partial F_e}{\partial p_\theta} + \frac{\partial \psi}{\partial \phi} \frac{\partial F_e}{\partial p_\phi} = 0. \quad (17)$$

The first term is antisymmetric in  $p_r$ , whereas all other terms are symmetric. So, it must be the case that  $F_e$  does not depend on  $r$ . (This is analogous to the elimination of the nodes in the  $N$ -body problem which similarly reduces the order of the system in phase space by two – see e.g. Boccaletti & Pucacco 1996.)

We now multiply by  $r^2$  and differentiate with respect to  $r$  at constant  $H, p_\theta, p_\phi, \theta, \phi$  to obtain

$$\frac{\partial F_e}{\partial p_\theta} \frac{\partial^2}{\partial r \partial \theta} (r^2 \psi) + \frac{\partial F_e}{\partial p_\phi} \frac{\partial^2}{\partial r \partial \phi} (r^2 \psi) = 0. \quad (18)$$

The first term is odd with respect to  $p_\theta$ , the second term odd with respect to  $p_\phi$ . However, the equation must remain true under  $p_\theta \rightarrow -p_\theta$  or  $p_\phi \rightarrow -p_\phi$ , and so each term must separately vanish.

There are four possibilities – either (case i)

$$\frac{\partial F_e}{\partial p_\phi} = 0 = \frac{\partial F_e}{\partial p_\theta}, \quad (19)$$

or case (ii)

$$\frac{\partial F_e}{\partial p_\theta} = 0 = \frac{\partial^2}{\partial r \partial \phi} (r^2 \psi), \quad (20)$$

or case (iii)

$$\frac{\partial F_e}{\partial p_\phi} = 0 = \frac{\partial^2}{\partial r \partial \theta} (r^2 \psi), \quad (21)$$

or case (iv)

$$\frac{\partial^2}{\partial r \partial \phi} (r^2 \psi) = 0 = \frac{\partial^2}{\partial r \partial \theta} (r^2 \psi), \quad (22)$$

cases (i)–(iii) lead to the degenerate cases in which two or three of the semiaxes of the second velocity moment ellipsoid are the same. For example, case (i) tells us that  $F_e$  is independent of both  $p_\theta$  and  $p_\phi$ . On returning to equation (17), we see that it also follows that  $F_e$  is independent of the conjugate coordinates  $\theta$  and  $\phi$  as well, leaving us with  $F_e = F_e(H)$ , or solutions with completely isotropic velocity ellipsoids. The other degenerate cases are when the DF is given by  $F_e = F_e(H, |\mathbf{L}|)$  in a spherical potential, or  $F_e = F_e(E, L_z)$  in an axisymmetric potential. Here,  $\mathbf{L}$  is the angular momentum, whilst  $L_z$  is the component of  $\mathbf{L}$  that is parallel to the symmetry axis. Both lead to the second velocity moment ellipsoid possessing axial symmetry – in the former case with  $\langle v_r^2 \rangle = \langle v_\theta^2 \rangle$ , in the latter case with  $\langle v_r^2 \rangle = \langle v_\phi^2 \rangle$ . These models have been known since at least the Adams Prize essay of James Jeans (1919). However, it has also long been known that the velocity ellipsoid of Milky Way halo stars is triaxial with  $\langle v_r^2 \rangle > \langle v_\phi^2 \rangle > \langle v_\theta^2 \rangle$  (see e.g. Woolley 1978; Chiba & Beers 2000; Képley et al. 2007; Smith et al. 2009a; Bond et al. 2010). Therefore, the degenerate instances of spherical alignment do not seem to apply to the case of the Milky Way stellar halo anyhow.

Only case (iv) survives. The solution to  $\partial^2(r^2 \psi)/\partial r \partial \theta = 0$  is

$$r^2 \psi = A(r, \phi) + B(\theta, \phi), \quad (23)$$

where  $A(r, \phi)$  and  $B(\theta, \phi)$  are arbitrary functions of the indicated arguments. If we also demand that  $\partial^2(r^2 \psi)/\partial r \partial \phi = 0$ , then we have

$$\frac{\partial^2 A}{\partial r \partial \phi} = 0 \Rightarrow A = A_1(r) + A_2(\phi), \quad (24)$$

where  $A_1(r)$  and  $A_2(\phi)$  are again arbitrary. Thus absorbing  $A_2$  into a new function  $A_3(\theta, \phi)$ , we obtain the result

$$\psi = \frac{A_1(r)}{r^2} + \frac{A_2(\theta, \phi)}{r^2} = \psi_1(r) + \frac{A_2(\theta, \phi)}{r^2}, \quad (25)$$

where  $\psi_1(r) = A_1(r)/r^2$  and  $A_2(\theta, \phi)$  is an arbitrary function. So, the radial coordinate separates from the other coordinates. This means that there is an additional integral of the motion by separation of the Hamilton–Jacobi equation:

$$I = \frac{1}{2} \left( p_\theta^2 + \frac{p_\phi^2}{\sin^2 \theta} \right) - A_2(\theta, \phi). \quad (26)$$

So, we can additionally replace  $p_\theta^2$  with  $I$  in the DF, which means that  $F_e = F_e(H, I, p_\phi^2, r, \theta, \phi)$ . Taking the Poisson bracket and exploiting the fact that both  $H$  and  $I$  may be taken as constants during the differentiation, we deduce that  $F_e$  must now be independent of both  $r$  and  $\theta$ , and so are just left with

$$\frac{p_\phi}{r^2 \sin^2 \theta} \frac{\partial F_e}{\partial \phi} + \frac{\partial \psi}{\partial \phi} \frac{\partial F_e}{\partial p_\phi} = 0. \quad (27)$$

Multiplying through by  $\sin^2\theta$  and differentiating with respect to  $\theta$  gives

$$\frac{\partial^2}{\partial\theta\partial\phi}(\sin^2\theta\psi) = 0. \quad (28)$$

Inserting equation (25) into equation (28), this leads to the separable or Stäckel potential in spherical polars, namely

$$\psi = \psi_1(r) + \frac{\psi_2(\theta)}{r^2} + \frac{\psi_3(\phi)}{r^2\sin^2\theta}, \quad (29)$$

where  $\psi_2(\theta)$  and  $\psi_3(\phi)$  are arbitrary functions. This is the result claimed by Smith et al. (2009b); namely, that if the second velocity moment ellipsoid is aligned everywhere in spherical polar coordinates, then the only non-singular potential is spherically symmetric. It is worth emphasizing the very general nature of the assumptions required to deduce the result. Nothing about the quadratic nature of the integrals or the separability of the underlying potential has been assumed. Rather, these are logical consequences that follow from the assumption of spherical alignment. This proof follows the outline of the one presented in Smith et al. (2009b), amplifying the working where necessary. It differs in one respect. Smith et al. (2009b) assumed that  $\langle v_r \rangle = 0$  implies that the DF depends on  $v_r^2$ . This though is not necessarily true.

Note too that for the purposes of the theorem, it is immaterial whether the population self-consistently generates the gravitational field or not. The result holds good for tracer populations moving in an externally imposed potential, as well as populations that generate the gravity field in which they move. Finally, although the singularities in the potentials (25) or (29) at  $r = 0$  may seem objectionable, we show in Appendix A that this awkwardness can sometimes be avoided.

## 4 OTHER ALIGNMENTS

Other alignments of the second velocity moment ellipsoid are also of interest in galactic astronomy and dynamics. Here, we consider cylindrical and spheroidal alignment in some detail. From our work on spherical alignment, we may conjecture that the only possible solutions for triaxial velocity ellipsoids are the separable or Stäckel potentials. We now demonstrate that such is indeed true.

### 4.1 Cylindrical alignment

This case is interesting because it has implications for the popular JAM models introduced by Cappellari (2008), which assume cylindrical alignment. In JAM, the only non-vanishing components of the second velocity moment tensor are  $\langle v_R^2 \rangle$ ,  $\langle v_\phi^2 \rangle$  and  $\langle v_z^2 \rangle$ . JAM models assume a fixed anisotropy  $\beta_z = \langle v_z^2 \rangle / \langle v_R^2 \rangle$ . Using the boundary conditions that the velocity moments vanish at infinity then leads to an elegant way of solving the Jeans equations for the velocity dispersion as quadratures.

We take as our starting point the fact that the second velocity moment ellipsoid is aligned with the cylindrical polar coordinate system so that all the cross terms  $\langle v_R v_\phi \rangle = \langle v_z v_\phi \rangle = \langle v_R v_z \rangle$  vanish. As before, we take the even part of the DF to be  $F_e = F_e(p_R^2, p_\phi^2, p_z^2, r, \phi, z)$ , where the canonically conjugate momenta are  $p_R = v_R$ ,  $p_\phi = Rv_\phi$  and  $p_z = v_z$ . The Hamiltonian is

$$H = \frac{1}{2} \left( p_R^2 + \frac{p_\phi^2}{R^2} + p_z^2 \right) - \psi(R, \phi, z), \quad (30)$$

where  $\psi$  is the gravitational potential. The even part of the DF can now be recast as  $F_e(p_R^2, p_\phi^2, H, R, \phi, z)$  by using the Hamiltonian

to eliminate  $p_z^2$ . The  $H$  in the DF may be treated as a constant when evaluating the derivatives in the Poisson bracket, yielding

$$\begin{aligned} p_R \frac{\partial F_e}{\partial R} + \frac{p_\phi}{R^2} \frac{\partial F_e}{\partial \phi} + p_z \frac{\partial F_e}{\partial z} \\ + \left( \frac{p_\phi^2}{R^3} + \frac{\partial \psi}{\partial R} \right) \frac{\partial F_e}{\partial p_R} + \frac{\partial \psi}{\partial \phi} \frac{\partial F_e}{\partial p_\phi} = 0. \end{aligned} \quad (31)$$

As only the third term involves  $p_z$ , it follows that  $\partial F_e / \partial z = 0$  and so  $F_e$  must also be independent of  $z$ . Now differentiate with respect to  $z$  to obtain

$$\frac{\partial F_e}{\partial p_R} \frac{\partial^2 \psi}{\partial R \partial z} + \frac{\partial F_e}{\partial p_\phi} \frac{\partial^2 \psi}{\partial \phi \partial z} = 0 \quad (32)$$

The first term is odd with respect to  $p_R$ , the second term odd with respect to  $p_\phi$ . Hence, for this to be generally true, each term must separately vanish.

There are again four possibilities – either (case i)

$$\frac{\partial F_e}{\partial p_R} = 0 = \frac{\partial F_e}{\partial p_\phi}, \quad (33)$$

or case (ii)

$$\frac{\partial F_e}{\partial p_R} = 0 = \frac{\partial^2 \psi}{\partial \phi \partial z}, \quad (34)$$

or case (iii)

$$\frac{\partial F_e}{\partial p_\phi} = 0 = \frac{\partial^2 \psi}{\partial R \partial z}, \quad (35)$$

or case (iv)

$$\frac{\partial^2 \psi}{\partial \phi \partial z} = 0 = \frac{\partial^2 \psi}{\partial R \partial z} \quad (36)$$

As before, cases (i)–(iii) provide the degenerate solutions in which one or more of the second velocity moments is everywhere the same. This leaves case (iv), which is non-degenerate and  $\langle v_R^2 \rangle$ ,  $\langle v_\phi^2 \rangle$  and  $\langle v_z^2 \rangle$  are all unequal, as the general case. Solving  $\partial^2 \psi / \partial \phi \partial z = 0$  is

$$\psi = A(R, \phi) + B(R, z), \quad (37)$$

where  $A(R, \phi)$  and  $B(R, z)$  are arbitrary functions of the indicated arguments. When we also demand that  $\partial^2 \psi / \partial R \partial z = 0$ , then we have

$$\psi(R, \phi, z) = A(R, \phi) + \psi_3(z), \quad (38)$$

where  $\psi_3(z)$  is an arbitrary function. Notice that we have now proved that the  $z$  component separates from the other coordinates, and that the energy in the  $z$  direction  $H_z$

$$H_z = \frac{1}{2} p_z^2 - \psi_3(z), \quad (39)$$

is an integral of motion.

Of course, we can now repeat our calculation by recasting the even part of the DF as  $F_e(H, p_\phi^2, H_z, R, \phi, z)$  using the Hamiltonian  $H$  to eliminate  $p_R^2$  and  $H_z$  to eliminate  $p_z^2$ . Again taking the Poisson bracket  $\{F_e, H\} = 0$ , we straightforwardly establish that  $F_e$  must be independent of the conjugate coordinates  $R$  and  $z$ , and are left with

$$\frac{p_\phi}{R^2} \frac{\partial F_e}{\partial \phi} + \frac{\partial \psi}{\partial \phi} \frac{\partial F_e}{\partial p_\phi} = 0. \quad (40)$$

Multiplying through by  $R^2$  and differentiating with respect to  $R$  gives

$$\frac{\partial^2(R^2\psi)}{\partial R\partial\phi} = 0. \quad (41)$$

So, using equation (38), the final solution for the potential is

$$\psi = \psi_1(R) + \frac{\psi_2(\phi)}{R^2} + \psi_3(z), \quad (42)$$

where  $\psi_1(R)$  and  $\psi_2(\phi)$  are arbitrary. This is the separable or Stäckel potential in cylindrical polars (see e.g. Landau & Lifshitz 1976; Goldstein 1980).

Of course, it has long been known that if the potential is separable in cylindrical polars, then the second velocity moment ellipsoid is aligned in the cylindrical polar coordinate system. What has been proved here for the first time is the converse. If the second velocity moment ellipsoid is non-degenerate and aligned in cylindrical polar coordinates, then the gravitational potential is separable or Stäckel in cylindrical polar coordinates. The degenerate cases are the ones in which at least two of the semiaxes are everywhere the same, and so correspond to models with DFs that have  $F(E)$  (isotropic DFs),  $F(E, L_z)$  (axisymmetric potential) and  $F(E, E_z)$  (translationally invariant potential).

What then is the status of the JAM models of Cappellari (2008)? The Jeans solutions are cylindrically aligned with (in general) three unequal axes. If the even part of the velocity distributions is symmetric (i.e. invariant under  $v_R \rightarrow -v_R$ ,  $v_\phi \rightarrow -v_\phi$  and  $v_z \rightarrow -v_z$ ), then the only such physical models must have potentials that separate in the cylindrical polar coordinate system. Unfortunately, this yields through Poisson's equation a total matter density of the form

$$\rho(R, \phi, z) = \rho_1(R) + \frac{\rho_2(\phi)}{R^4} + \rho_3(z). \quad (43)$$

The fact that the density separates into stratified layers in  $z$  with the same profile in  $(R, \phi)$  makes this unrealistic for all known astrophysical objects. For arbitrary and astrophysically realistic potentials, the JAM models are unlikely to be physical. The only loophole is if the even part of the DF does not fulfil the symmetry requirement. This is shown by An & Evans (2016) to be equivalent to requiring the fourth moments  $\langle v_R v_\phi^3 \rangle$ ,  $\langle v_\phi^3 v_z \rangle$ ,  $\langle v_R^3 v_\phi \rangle$ ,  $\langle v_R^2 v_\phi v_z \rangle$ ,  $\langle v_R v_\phi v_z^3 \rangle$  and  $\langle v_\phi v_z^3 \rangle$  not to all vanish.

We advocate exercising care in the use of JAM solutions because the alignment also seems unnatural (except perhaps in the central parts of elliptical galaxies). Physically, we expect astrophysical objects to be at least roughly aligned in spherical polar coordinates rather than cylindrical, as is borne out by our investigations of the stellar halo. Probably, it makes sense to use the JAM solutions for preliminary models only before they are elaborated upon with Schwarzschild (Schwarzschild 1979) or Made-To-Measure methods (Syer & Tremaine 1996; Dehnen 2009).

## 4.2 Spheroidal alignment

It is straightforward to generalize the proof to the instance of axisymmetric stellar systems with second velocity moments aligned in spheroidal coordinates  $(\lambda, \mu, \phi)$ . This coordinate system has been introduced in equation (13) and is described in detail in, for example, Morse & Feshbach (1953) or Binney & Tremaine (2008). Here, we will show that if the second velocity moment ellipsoid is everywhere aligned in spheroidal coordinates ( $\langle v_\lambda v_\phi \rangle = \langle v_\lambda v_\mu \rangle = \langle v_\mu v_\phi \rangle = 0$ ), then the gravitational potential has Stäckel or separable form. Again, we construct the even part of the DF. Introducing canonical coordi-

nates, the DF has the form  $F_e(p_\lambda^2, p_\mu^2, p_\phi^2, \lambda, \mu, \phi)$ . The Hamiltonian is

$$H = \frac{1}{2} \left( \frac{p_\lambda^2}{P^2} + \frac{p_\mu^2}{Q^2} + \frac{p_\phi^2}{R^2} \right) - \psi(\lambda, \mu, \phi), \quad (44)$$

where the scale factors are  $P, Q$  and  $R$  are

$$P^2 = \frac{\lambda - \mu}{4(\lambda + a)(\lambda + b)}, \quad Q^2 = \frac{\mu - \lambda}{4(\mu + a)(\mu + b)}, \quad (45)$$

$$R^2 = \frac{(\lambda + a)(\mu + a)}{a - b},$$

and  $a$  and  $b$  are constants (see for example the tables of Lynden-Bell 1962 or equation (6) of Evans & Lynden-Bell 1989 or Section 2 of de Zeeuw 1985). This implies that the DF can be re-written as  $F_e(H, p_\mu^2, p_\phi^2, \lambda, \mu, \phi)$ . Just as before, requiring the Poisson bracket  $\{H, F_e\}$  to vanish implies that  $\partial F_e / \partial \lambda$  also vanishes and so  $F_e$  is independent of  $\lambda$ . This leaves us with the condition

$$A \frac{\partial F_e}{\partial p_\mu} - \frac{\partial \psi}{\partial \phi} \frac{\partial F_e}{\partial p_\phi} = \frac{p_\mu}{Q^2} \frac{\partial F_e}{\partial \mu} + \frac{p_\phi}{R^2} \frac{\partial F_e}{\partial \phi} \quad (46)$$

with

$$A = \frac{1}{\lambda - \mu}$$

$$\left[ \frac{p_\mu^2}{2} \frac{\partial}{\partial \mu} \left( \frac{\lambda - \mu}{Q^2} \right) + \frac{p_\phi^2}{2} \frac{\partial}{\partial \mu} \left( \frac{\lambda - \mu}{R^2} \right) - \frac{\partial}{\partial \mu} ((\lambda - \mu)\psi) + H \right]. \quad (47)$$

Again, the equation must hold on transforming  $p_\mu \rightarrow -p_\mu$ , so that in the general case (i.e. ignoring degenerate cases like isotropy), we must have

$$A \frac{\partial F_e}{\partial p_\mu} = \frac{p_\mu}{Q^2} \frac{\partial F_e}{\partial \mu}, \quad \frac{\partial \psi}{\partial \phi} \frac{\partial F_e}{\partial p_\phi} = \frac{p_\phi}{R^2} \frac{\partial F_e}{\partial \phi}. \quad (48)$$

Multiplying the first equation by  $\lambda - \mu$ , differentiating with respect to  $\lambda$  at constant  $H$  and then using the definitions of the scale factors gives us the simple result

$$\frac{\partial^2}{\partial \lambda \partial \mu} ((\lambda - \mu)\psi) = 0. \quad (49)$$

Integrating up, this gives us

$$\psi = \frac{A(\lambda, \phi) - B(\mu, \phi)}{\lambda - \mu}, \quad (50)$$

where  $A(\lambda, \phi)$  and  $B(\mu, \phi)$  are arbitrary.

Now, we can return to the beginning and instead of eliminating  $p_\lambda^2$  in terms of  $H$ , we can eliminate  $p_\phi^2$  so that the DF is  $F_e(p_\lambda^2, p_\mu^2, H, \lambda, \mu, \phi)$ . Repeating the steps gives us

$$\frac{\partial^2}{\partial \lambda \partial \phi} (R^2\psi) = \frac{\partial^2}{\partial \mu \partial \phi} (R^2\psi) = 0, \quad (51)$$

from which on inserting equation (50), we obtain the separable or Stäckel potential in spheroidal coordinates

$$\psi = \frac{f_1(\lambda) - f_2(\mu)}{\lambda - \mu} + \frac{f_3(\phi)}{R^2}, \quad (52)$$

with  $f_1(\lambda)$ ,  $f_2(\mu)$  and  $f_3(\phi)$  arbitrary functions of indicated arguments. Of course, these potentials have a long history in both classical mechanics (e.g. Levi-Civita 1904; Whittaker 1917; Weinacht 1924; Eisenhart 1934, 1948) and stellar dynamics (e.g. Eddington 1915; Clark 1937; Lynden-Bell 1962). In astrophysical applications, it is usual to set  $f_3(\phi) = 0$  as otherwise the gravitational

potential diverges on the axis  $R = 0$ . de Zeeuw (1985) provided examples – now known as the perfect oblate or prolate spheroids – of realistic self-gravitating stellar systems with density stratified on similar concentric spheroids that have a potential of Stäckel form. The models are important, as their orbital structure is generic (see e.g. Boccaletti & Pucacco 1996; Binney & Tremaine 2008).

It has been known for many years that, in the axisymmetric Stäckel potentials, the second velocity moment ellipsoid is aligned in spheroidal coordinates (e.g. Lynden-Bell 1960; de Zeeuw 1985; Evans & Lynden-Bell 1989). We have shown here the converse also holds true. If the velocity ellipsoid is spheroidally aligned everywhere and the even part of the DF symmetric under  $v_\lambda \rightarrow -v_\lambda$ ,  $v_\phi \rightarrow -v_\phi$  and  $v_\mu \rightarrow -v_\mu$ , then the potential must be of separable or Stäckel form.

Spherical polar, cylindrical polar and spheroidal coordinates are all limits of the most general case, ellipsoidal coordinates (Morse & Feshbach 1953). It may well be suspected that the theorem holds true for ellipsoidal coordinates as well. Such is indeed true, but we relegate details of this, the most cumbersome case, to Appendix B. Finally, it is also reasonable to suspect that a general proof can be found, irrespective of the coordinate system. In Appendix C, we show that just the assumption of a triaxial velocity ellipsoid aligned everywhere in some orthogonal coordinate system, together with the existence of a steady-state DF with symmetries in velocity space, is sufficient to constrain the system to be Stäckel in ellipsoidal coordinates, or one of its limits (see also An & Evans 2016). Although this material has been placed in an appendix as it is somewhat mathematical, none the less we regard it as a more powerful proof of Eddington’s (1915) theorem which does not rest on the so-called ‘ellipsoidal hypothesis’, namely the assumption that the DF depends on a single quadratic function of the velocities (see e.g. Chandrasekhar 1942 and Cubarsi 2014 for later work on the ellipsoidal hypothesis).

## 5 MADE-TO-MEASURE MODELS OF THE STELLAR HALO

Theorems on exact alignment are interesting, but in practice the alignment is approximate and the data extend only over high latitude fields that are comparatively nearby. Is it possible to build models in which the alignment is close to spherical, but the gravitational potential is flattened?

To investigate this, we use a made-to-measure method to construct a triaxial stellar halo tracer population in a potential generated by a triaxial NFW dark matter halo. We utilize the made-to-measure code of Dehnen (2009, hereafter D09). The construction of this model follows very closely the construction of the models presented in D09 and here we only briefly describe the made-to-measure method.

The made-to-measure technique was pioneered by Syer & Tremaine (1996). In their formulation, an equilibrium model is constructed by evolving an  $N$ -body simulation whilst simultaneously adjusting the particle weights until a merit function is optimized. The merit function is expressed as

$$Q = \mu S - \frac{1}{2}C, \quad (53)$$

where  $C$  is a cost function that quantifies the deviation of the model from our target model (for instance, the  $\chi^2$  difference between the model moments and the target moments) and  $S$  is an entropy term that regularizes the weight distribution of the particles. The  $N$ -body simulation is evolved whilst each particle weight  $w_i$  is adjusted

according to a first-order differential equation that maximises the merit function  $Q$ . One difficulty encountered by Syer & Tremaine (1996) is that the cost function naturally fluctuates as the simulation is evolved due to Poisson noise, so some form of smoothing is required to ensure the algorithm converges. D09 pointed out that Syer & Tremaine’s method of simply averaging the model properties used in the cost function did not ensure the model converged, so D09 instead proposed smoothing the merit function  $Q$  by making the weight-adjustment equation a second-order differential equation. Several other improvements to the original algorithm were presented by D09. In his formulation (i) each particle is evolved on its own dynamical time-scale such that the outer parts of the model converge as rapidly as the inner regions, (ii) a total weight constraint is included as part of the merit function and (iii) the particles are resampled when the ratio between the minimum and maximum weight (normalized with respect to the priors) exceeds a chosen value. The last of these is implemented by, every so often, drawing new particles from the original set with probability proportional to their prior-normalized weights and adding a random velocity offset with a magnitude that declines exponentially as a function of the simulation time. For the model presented below we use very similar parameters for the algorithm as those presented in D09.

Using the made-to-measure method, we construct an equilibrium tracer stellar population inside a fixed dark matter potential. The density profile of both the dark matter and the tracer population is given by a truncated double power law of the form

$$\rho_i \propto \left(\frac{q_i}{r_{0,i}}\right)^{-\gamma_i} \left[1 + \left(\frac{q_i}{r_{0,i}}\right)\right]^{(\gamma_i - \beta_i)} \operatorname{sech}\left(\frac{q_i}{r_{t,i}}\right), \quad (54)$$

where  $r_{0,i}$  is the scale radius of the  $i$ th component,  $r_t$  the truncation radius and the elliptical radius  $q$  is defined as

$$q_i^2 = \frac{x^2}{a_i^2} + \frac{y^2}{b_i^2} + \frac{z^2}{c_i^2}, \quad (55)$$

with  $a_i b_i c_i = 1$ . We choose the parameters for the NFW halo as  $\gamma_{\text{NFW}} = 1$ ,  $\beta_{\text{NFW}} = 3$ ,  $(b/a)_{\text{NFW}} = 0.9$ ,  $(c/a)_{\text{NFW}} = 0.8$ ,  $r_{0,\text{NFW}} = r_0$  and  $r_{t,\text{NFW}} = 10r_0$ , whilst the target stellar halo has  $\gamma_S = 1$ ,  $\beta_S = 4.5$ ,  $(b/a)_S = 0.8$ ,  $(c/a)_S = 0.6$ ,  $r_{0,S} = 1.73r_0$  and  $r_{t,S} = 9r_0$ . These choices are motivated by several studies of the halo. In the dynamical models of Piffil et al. (2014), the NFW dark matter halo was found to have a scale radius of  $r_0 = 15.5$  kpc, where the constraint comes mostly from the mass measurements of Wilkinson & Evans (1999) and the requirement that the halo lies on the mass–concentration relation. Deason, Belokurov & Evans (2011) found from a population of BHB stars that the stellar halo had a scale radius of  $r_{0,S} = 27$  kpc and a flattening  $(c/a)_S = 0.59$ . The axis ratios of the NFW profile are representative of those found in cosmological simulations (see for example Bryan et al. 2013).

The cost function corresponding to this density profile is given by

$$C_\rho = \sum_n \left(\frac{A_n - B_n}{\sigma_n}\right)^2, \quad (56)$$

where  $A_n$  is the dot product of the model potential with the  $\mathbf{n}^{\text{th}} = (n, l, m)^{\text{th}}$  basis function of the Zhao (1996) basis set chosen to match the outer slope of the target model, and  $B_n$  is the corresponding target moment with  $\sigma_n$  an estimate of the error in the moment calculated from the variance of 100 realizations of the target model. We set  $n_{\text{max}} = 20$  and  $l_{\text{max}} = 12$  such that 588 moments are used to describe the density. Similarly, the potential used to describe the NFW halo is represented as a basis function

expansion generated from a single sample of the density distribution.  $10^6$  particles were used for each realization of the stellar halo and  $10^8$  for realization of the dark matter density distribution. The total mass of the NFW halo is  $M$  and the stellar halo is treated purely as a tracer population.

Additionally, we impose an anisotropy profile for the tracer population as

$$\beta(q) = 1 - \frac{\sigma_\theta^2 + \sigma_\phi^2}{2\sigma_r^2} = \frac{\beta_0 + \beta_\infty(q/r_0)}{1 + (q/r_0)} \quad (57)$$

which goes from  $\beta_0$  at small radii to  $\beta_\infty$  at large radii over a scale  $r_0$ . We choose  $\beta_0 = 0$  and  $\beta_\infty = 0.75$  which approximates the form for the anisotropy found by Williams & Evans (2015). The corresponding cost function  $C_\beta$  is the  $\chi^2$  deviation of the model anisotropy from the target calculated in elliptical shells with the same shape as the target density. The error is estimated as the Poisson noise arising from a measurement of the anisotropy from samples of an uncorrelated normal velocity distribution.

The initial  $N$ -body model is chosen to be the ergodic model with the required radial density profile, that is then flattened by the appropriate axis ratios and the velocities scaled to satisfy the tensor virial theorem. We began by running this model for 200 time units subject to the density constraints. The model converged within  $\sim 50$  time units and subsequent evolution with the weight adjustment switched off did not cause the model to deviate significantly from the target distribution. The anisotropy of this model was increased from weakly radial ( $\beta \sim 0.2$ ) at  $0.1r_0$  to more strongly radial ( $\beta \sim 0.5$ ) at  $r = r_{t,S}$ . We then proceeded to evolve the model further subject also to the anisotropy constraint. The model converged within  $\sim 30$  time units and again did not deviate from the target under subsequent evolution with no weight adjustment.

The resulting simulation is plotted in Fig. 6. In Figs 7–9, we show the velocity ellipses in the principal planes of the potential along with the misalignment from spherical alignment. In all three principal planes, the velocity ellipsoid is misaligned from spherical by  $\lesssim 6^\circ$  everywhere outside the scale radius of the stellar halo. Inside the scale radius, there are also large regions where the misalignment is  $\lesssim 6^\circ$  with the largest misalignments occurring at small  $x$  and small  $z$  as well as small  $x$  and small  $y$ . However, inspecting the velocity ellipses in these regions shows they are very round and so the misalignment measurement is more susceptible to shot noise. To inspect the impact of shot noise in the measurement of the tilt from the simulation we show  $\alpha/\sigma_\alpha$  in the  $(x, y)$  plane in Fig. 10.  $\sigma_\alpha$  was computed using propagation of errors from the measured dispersions. We see that the majority of the plane is consistent with being aligned within the shot noise. This plane is representative of the other two principal planes and similar to the simulations shown later. We conclude we are not dominated by shot noise from the simulation when drawing conclusions on the degree of alignment. Instead when comparing these models with the data we are limited by the errors in the observational data.

For the simulation without the anisotropy constraint, we also found that there were large regions of spherical alignment particularly outside the scale radius in the  $(y, z)$  plane and along the  $x$ -axis. However, near the  $y$ - and  $z$ -axis the ellipses became more circular with the suggestion that a minor axis is aligned with spherical polars. Increasing the anisotropy has the effect of increasing the volume in which the major axis of the velocity ellipsoid is spherically aligned. We are able to produce a realistic model of the stellar halo in a triaxial NFW halo that has a large volume in which that velocity ellipsoid is aligned with spherical polars within  $\sim 6^\circ$ .

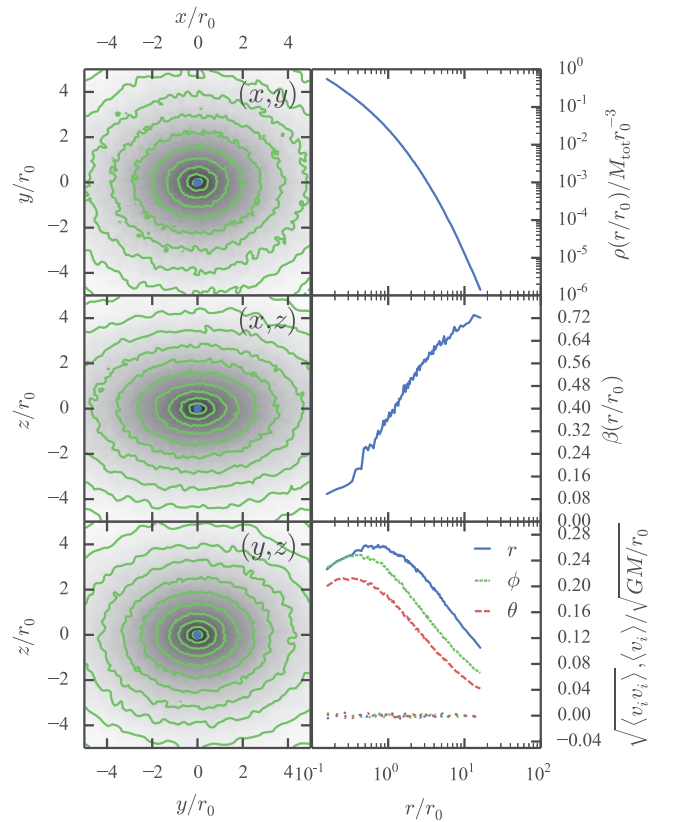


**Figure 6.** Made-to-measure stellar halo properties: the left-hand panels show the density integrated along the line of sight in the three principal planes. The green contours are evenly spaced in logarithmic density and the blue point is the centre of mass. The top-right panel shows the spherically averaged density profile, the middle right panel the spherically averaged anisotropy profile and the bottom-right panel the spherically averaged velocity dispersions and mean velocities. Note all the mean velocities are zero, as there is no net streaming.

The constructed model has a fairly round potential due to the only weakly triaxial NFW density profile for the dark matter. To investigate whether the alignment persists for a flatter model, we now go on to construct a model with  $(b/a)_{\text{NFW}} = 0.7$ ,  $(c/a)_{\text{NFW}} = 0.5$ ,  $(b/a)_S = 0.65$  and  $(c/a)_S = 0.45$ . All other parameters are kept the same. In Figs 11–13, we show the corresponding velocity ellipses in the principal planes of the potential along with the misalignment from spherical polar coordinates. As expected, the region within which the alignment is less than  $\sim 6^\circ$  has decreased compared to the rounder model but there are still considerable regions, particularly outside  $q = r_S$ , where the alignment is spherical. Finally, we report that we constructed a model with  $(b/a)_{\text{NFW}} = 1$ ,  $(c/a)_{\text{NFW}} = 0.1$ ,  $(b/a)_S = 1$  and  $(c/a)_S = 0.5$ . This model has spherical alignment at very large radius ( $q > 6r_S$ ) and within  $q = r_S$  the long axis of the velocity ellipsoid is pointed more towards the plane for  $R > z$  and the short axis is pointed more towards the plane for  $z > R$ . However, it should be reported that this model appears to be only marginally stable as the cost functions drift in time upon subsequent evolution of the made-to-measure code with no weight adjustment. Our models do not include the majority of the baryons in the Galaxy (i.e. the disc) but based on our constructed models we can make some predictions as to the effects. Including a disc will cause the velocity ellipses to tilt slightly towards the plane. However, at large distances the disc potential is dominated by the monopole component such that this effect will be small for the majority of the volume studied

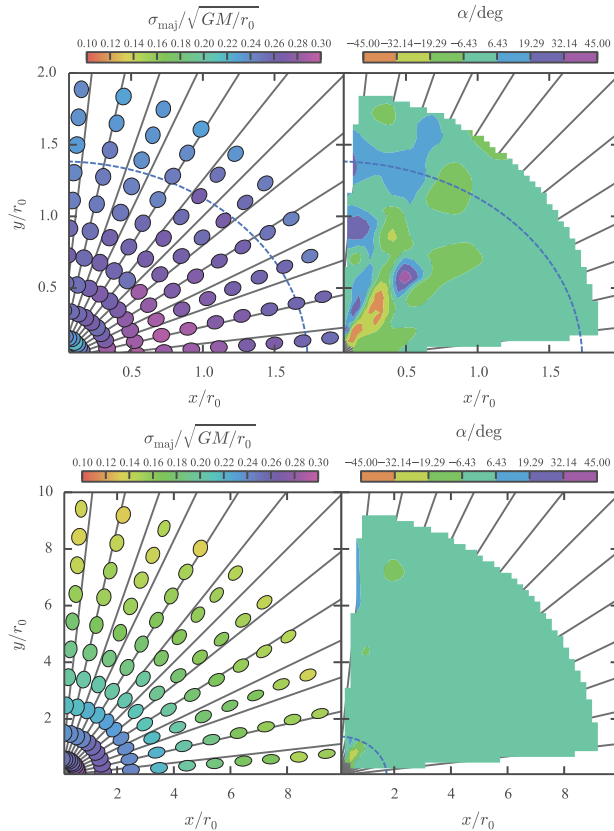


**Figure 7.** Tilt of the stellar halo for  $(b/a)_{\text{NFW}} = 0.9$ ,  $(c/a)_{\text{NFW}} = 0.8$  model in the  $(x, y)$  plane: the left-hand panels show the velocity ellipses coloured by the magnitude of their major axis. The size of the ellipses is unimportant and chosen for ease of visualization. The black lines are radial. The right-hand panels show the misalignment of the major axis of the ellipses from radial. The top two panels correspond to  $0 \lesssim r/r_0 < 2$  whilst the lower two correspond to  $0 \lesssim r/r_0 < 10$ . In all panels, the dotted blue line corresponds to  $q_S = r_0,S$ .

here. For example, both Koposov, Rix & Hogg (2010) and Bowden, Belokurov & Evans (2015) find a flattening for the full potential of  $q \sim 0.9$  when fitting the GD-1 stream which lies  $\sim 15$  kpc from the Galactic Centre so the models presented here are perhaps already too flattened *without* including the Galactic disc.

Notice that we did not introduce any requirement in the cost function (56) that drives the made-to-measure solutions to spherical alignment. We attempted to minimize the tilt angles from spherical alignment in spherical polar bins beyond a minimum elliptical radius but this produced no significant change to the structure of the models. It appears that the alignment cannot be significantly altered once the potential and tracer density have been specified. Making the models more radially anisotropic acts to make the alignment more obvious as the calculation of the tilt is less susceptible to Poisson noise. Flattened models with strong radial anisotropy seem to produce near-spherical alignment of the velocity ellipsoid in significant portions of configuration space without much difficulty. In other words, the inferred alignment of the velocity ellipsoid in relatively small spatial volumes does not constrain the Galactic potential. Strong inferences can be only made when global alignment is detected. Only with the advent of *Gaia* proper motions will we possess data sets of a large enough extent to use the velocity ellipsoid as a tool for inference on the symmetries of the Galactic matter distribution.

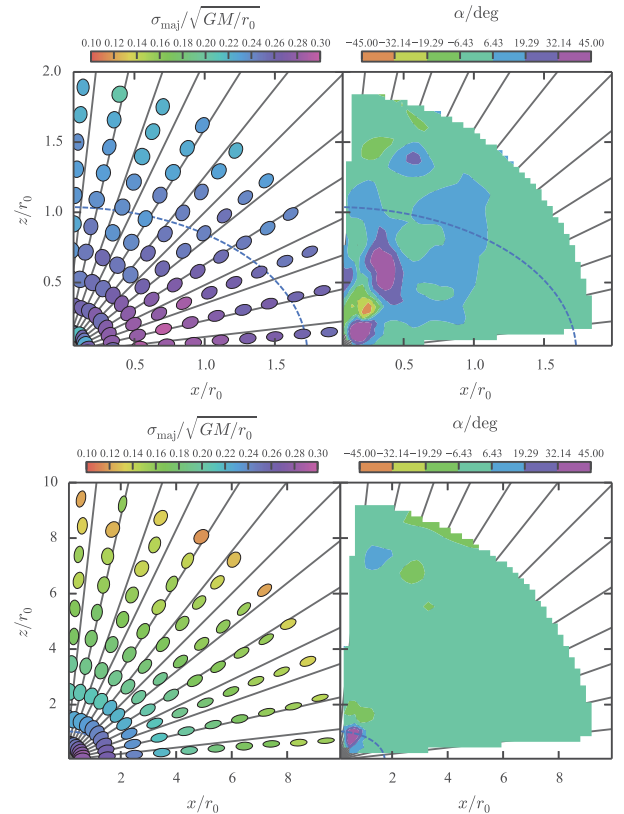


**Figure 8.** Tilt of the stellar halo for  $(b/a)_{\text{NFW}} = 0.9$ ,  $(c/a)_{\text{NFW}} = 0.8$  model in the  $(x, z)$  plane: see Fig. 7 for details.

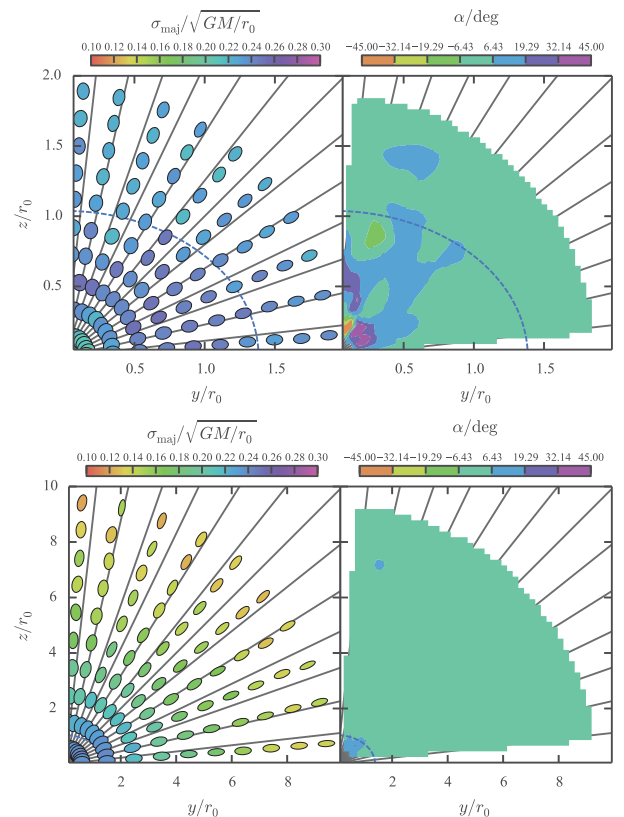


**Figure 9.** Tilt of the stellar halo for  $(b/a)_{\text{NFW}} = 0.9$ ,  $(c/a)_{\text{NFW}} = 0.8$  model in the  $(y, z)$  plane: see Fig. 7 for details.

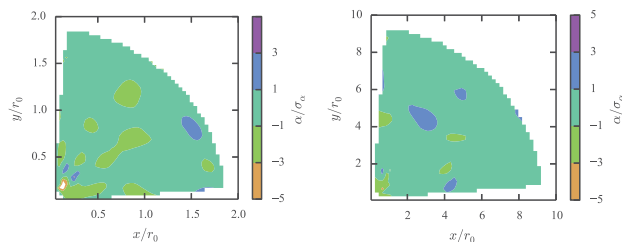


**Figure 10.** Tilt of the stellar halo divided by the error in the tilt for  $(b/a)_{\text{NFW}} = 0.9$ ,  $(c/a)_{\text{NFW}} = 0.8$  model in the  $(x, y)$  plane. The left-hand panel shows a zoom-in of the right-hand panel. The distributions in the other principal planes are very similar.

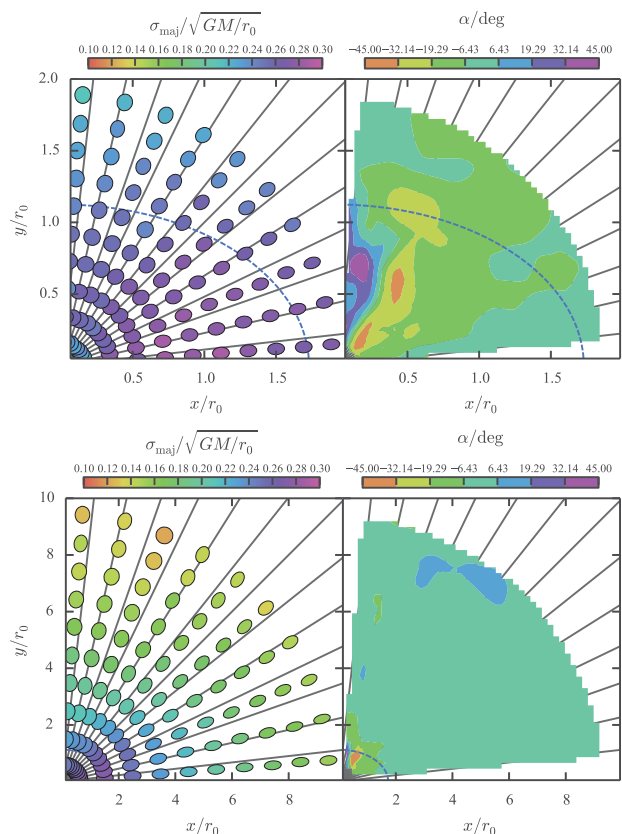


**Figure 11.** Tilt of the stellar halo tilt for flatter  $(b/a)_{\text{NFW}} = 0.7$ ,  $(c/a)_{\text{NFW}} = 0.5$  model in the  $(x, y)$  plane: see Fig. 7 for details.

## 6 CONCLUSIONS

This paper has identified the circumstances under which the second velocity moment tensor of a stellar population is everywhere aligned in the spherical polar coordinate system. Exact alignment in spherical polars is possible if (i) all three semiaxes are the same and the DF is isotropic, (ii) two of the semiaxes are the same ( $\langle v_r^2 \rangle = \langle v_\theta^2 \rangle$ ) and the potential is axisymmetric with a DF depending on the energy  $E$  and angular momentum parallel to the symmetry axis  $L_z$ , (iii) all three semiaxes are in general different and the potential is of separable or Stäckel form in spherical polar coordinates. In the latter instance, if the potential is everywhere non-singular, then it must be spherically symmetric. Our proof is based on the ideas sketched out in Smith et al. (2009b). An assumption in the proof is that the even part of the DF is symmetric under time reversal in each coordinate (i.e. under  $v_r \rightarrow -v_r$  or  $v_\theta \rightarrow -v_\theta$  or  $v_\phi \rightarrow -v_\phi$ ).

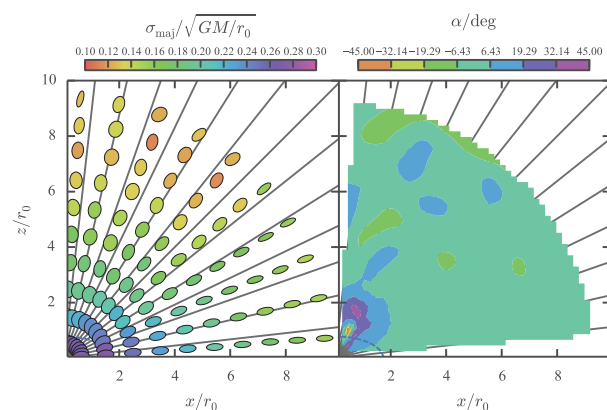
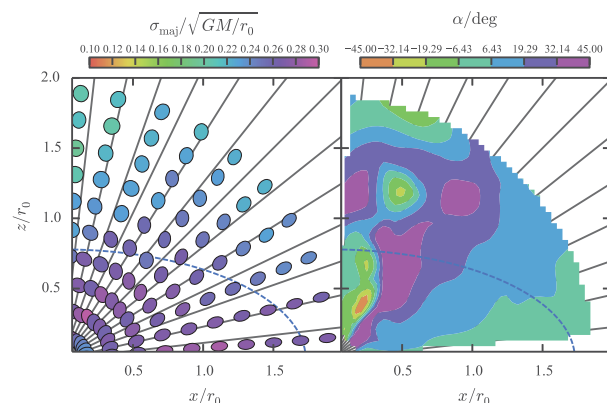


**Figure 12.** Tilt of the stellar halo for flatter  $(b/a)_{\text{NFW}} = 0.7$ ,  $(c/a)_{\text{NFW}} = 0.5$  model in the  $(x, z)$  plane: see Fig. 7 for details.

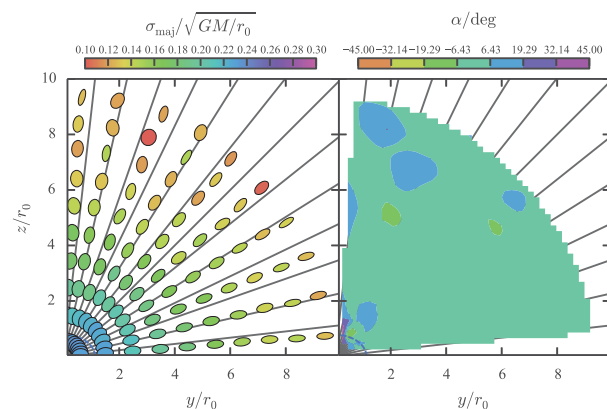
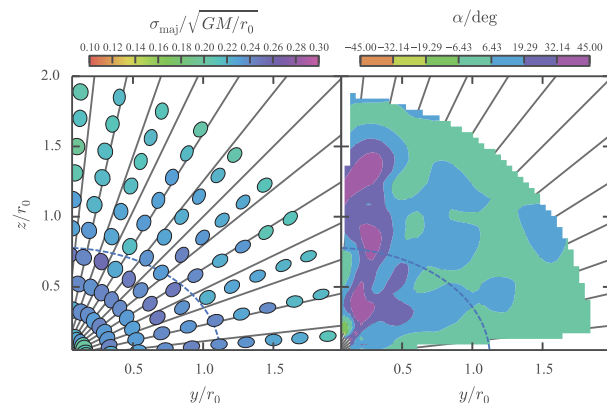


**Figure 13.** Tilt of the stellar halo tilt for flatter  $(b/a)_{\text{NFW}} = 0.7$ ,  $(c/a)_{\text{NFW}} = 0.5$  model in the  $(y, z)$  plane: see Fig. 7 for details.

We have shown that this theorem holds more generally. If the second velocity moment ellipsoid of a stellar system is triaxial and points along orthogonal coordinate surfaces, then the potential must be of separable or Stäckel form in confocal ellipsoidal coordinates or one of its limits. The converse of this theorem – namely, if the potential is of Stäckel form then the second velocity moment tensor aligns in the separable coordinate system – has been known since the time of Eddington (1915). In our proof, we emphasize that no assumption has been made about the form of the DF, or the existence of any integrals of the motion quadratic in the velocities. All we have assumed is that the even part of the DF remains invariant under the separate transformations  $v_i \rightarrow -v_i$  in each component (see also An & Evans 2016).

It is worth returning to Eddington’s (1915) work on the ellipsoidal hypothesis to spell out the differences. Eddington postulated the existence of integrals of motion that are quadratic in the velocities. The ellipsoidal hypothesis is the statement that the DF depends on a single linear combination of these integrals. Eddington then showed that the potential has to be of separable or Stäckel form and the velocity ellipsoid diagonalizes in the separating coordinates. However, integrals of the motion quadratic in the velocities only arise from separation of the Hamilton–Jacobi equation (see e.g. Makarov et al. 1967; Evans 1990). Hence, Eddington made an assumption of quadratic integrals that is tantamount to assuming the potential is of separable form in the first place.

One consequence of our theorem is that the elegant way of solving the Jeans equation for triaxial velocity ellipsoids using cylindrical polar alignment developed by Cappellari (2008) and known as ‘JAM modelling’ may only yield physical models if the potential is separable in the cylindrical polar coordinates. Unfortunately, this corresponds to total matter distributions that are unlike elliptical galaxies. If the potential is not of separable form in cylindrical polars, then there may be galaxy models with DFs that generate cylindrical alignment with triaxial second velocity moment tensors, though this however remains to be demonstrated. JAM models may make good provisional starting points for constructing  $N$ -body or made-to-measure models, but they are not trustworthy on their own. Even so, JAM models have had many successes in reproducing global properties like inclination and mass-to-light ratios in fast rotating ellipticals (Lablanche et al. 2012; Alf Drehmer et al. 2015).

What then are the consequences for the stellar halo of the Milky Way? Our theorem applies to stellar systems in which the velocity ellipsoid is spherically or spheroidally aligned everywhere. The data on halo stars of the Milky Way do suggest it is aligned with the spherical polar coordinate system (usually within  $3^\circ$ ) for Galactocentric radii between  $\sim 6$  and  $\sim 11$  kpc in the Northern hemisphere. There are one or two bins with more substantial deviations, though this may be partly a consequence of contamination by the thick disc at low latitude. We have also shown that alignment in prolate spheroidal coordinates does not give a markedly better fit than spherical alignment. In both calculations, no attempt has been made to remove substructure (such as Sagittarius stream stars or tidal debris) from the stellar halo sample. Such substructure is of course expected in  $\Lambda$  cold dark matter and might spoil any exact alignment for an underlying smooth halo population.

Binney & McMillan (2011) have argued that only limited inferences on the potential may be drawn from the orientation of the second velocity moment ellipsoid. They constructed DFs of the thin and thick discs of the Galaxy using orbital tori. They showed that at some locations above the plane in the vicinity of the Sun, the velocity ellipsoid is spherically aligned despite the matter distribution

being highly flattened. However, the more recent data on the stellar halo provided by Bond et al. (2010) does provide a more substantial challenge. Now the alignment is known to be almost spherical over a large swathe of the Galaxy, and it is unclear whether flattened models exist that can provide this.

To understand whether such approximate alignment is consistent with flattened or triaxial potentials, we have used made-to-measure modelling (Syer & Tremaine 1996; Dehnen 2009). We constructed a triaxial stellar halo tracer model in a triaxial NFW dark matter potential. The tracer population was chosen to be more triaxial ( $b/a = 0.8$ ,  $c/a = 0.6$ ) than the NFW profile ( $b/a = 0.9$ ,  $c/a = 0.8$ ). The stellar halo was chosen to have a double power-law density profile and an anisotropy profile that went from isotropic at the centre to very radial in the outskirts. Despite the triaxiality of the potential, it was found that the velocity ellipsoid had a major axis that deviated from spherical alignment by  $\lesssim 6^\circ$  for large regions of space. Outside the scale radius of the stellar halo, the velocity ellipsoid is nearly everywhere spherically aligned. We went on to investigate a model with a flatter NFW profile ( $b/a = 0.7$ ,  $c/a = 0.5$ ) and found that the volume of the spherical alignment region was decreased within the scale radius of the model although there were still considerable regions where the alignment was spherical.

If the alignment has to be exactly spherical everywhere, then the restriction on the potential is very severe. The potential has to be spherical if it is everywhere non-singular. However, if the alignment is only close to spherical over a substantial portion of configuration space, then a much greater variety of potentials are possible, including flattened ones. Strong inference on the potential can only be made if global spherical alignment is established. The *Gaia* satellite will provide six-dimensional phase space information for stars brighter than  $V \approx 20$  within 20 kpc of the Sun. This may provide data sets of sufficient global coverage to enable the alignment of the velocity ellipsoid to be used as a tool for constraining the Galactic potential.

## ACKNOWLEDGEMENTS

NWE thanks Zeljko Ivezić for stimulating him to think about this matter again, as well as providing data files and advice on the propagation of errors. JLS acknowledges the use of the PYTHON package PYNBODY (Pontzen et al. 2013) for the visualization of  $N$ -body snapshots. We thank an anonymous referee for a helpful report.

## REFERENCES

- Agnello A., Evans N. W., Romanowsky A. J., 2014, MNRAS, 442, 3284
- Alf Drehmer D., Storchi-Bergmann T., Ferrari F., Cappellari M., Riffel R. A., 2015, MNRAS, 450, 128
- An J. H., Evans N. W., 2011, MNRAS, 413, 1744
- An J. H., Evans N. W., 2016, ApJ, in press (arXiv:1509.09020)
- Arnold R., 1995, MNRAS, 276, 293
- Bacon R., 1985, A&A, 143, 84
- Bacon R., Simien F., Monnet G., 1983, A&A, 128, 405
- Binney J., 2014, MNRAS, 440, 787
- Binney J., McMillan P., 2011, MNRAS, 413, 1889
- Binney J., Merrifield M., 1998, Galactic Astronomy. Princeton Univ. Press, Princeton
- Binney J., Tremaine S., 2008, Galactic Dynamics, 2nd edn. Princeton Univ. Press, Princeton
- Boccaletti D., Pucacco G., 1996, Theory of Orbits 1: Integrable Systems and Non-Perturbative Methods. Springer-Verlag, Berlin
- Bond N. A. et al., 2010, ApJ, 716, 1
- Bowden A., Belokurov V., Evans N. W., 2015, MNRAS, 449, 1391

- Bramich D. M. et al., 2008, MNRAS, 386, 887
- Bryan S. E., Kay S. T., Duffy A. R., Schaye J., Dalla Vecchia C., Booth C. M., 2013, MNRAS, 429, 3316
- Cappellari M., 2008, MNRAS, 390, 71
- Cappellari M. et al., 2013, MNRAS, 432, 1709
- Chandrasekhar S., 1942, Principles of Stellar Dynamics. Univ. Chicago Press, Chicago, IL
- Chiba M., Beers T. C., 2000, AJ, 119, 2843
- Clark G. L., 1937, MNRAS, 97, 182
- Cretton N., de Zeeuw P. T., van der Marel R. P., Rix H.-W., 1999, ApJS, 124, 383
- Cubarsi R., 2014, A&A, 561, A141
- de Zeeuw T., 1985, MNRAS, 216, 273
- Deason A. J., Belokurov V., Evans N. W., 2011, MNRAS, 416, 2903
- Dehnen W., 2009, MNRAS, 395, 1079 (D09)
- Dehnen W., Gerhard O. E., 1993, MNRAS, 261, 311
- Eddington A. S., 1915, MNRAS, 76, 37
- Eisenhart L. P., 1934, Ann. Math., 35, 284
- Eisenhart L. P., 1948, Phys. Rev., 74, 87
- Evans N. W., 1990, Phys. Rev. A, 41, 5666
- Evans N. W., 2011, in Saikia D. J., Trimble V., eds, Fluid Flows to Black Holes: A Tribute to S Chandrasekhar on his Birth Centenary. World Scientific Press, Singapore, p. 137
- Evans N. W., Lynden-Bell D., 1989, MNRAS, 236, 801
- Evans N. W., Hafner R. M., de Zeeuw P. T., 1997, MNRAS, 286, 315
- Evans N. W., An J., Bowden A., Williams A. A., 2015, MNRAS, 450, 846
- Foreman-Mackey D., Hogg D. W., Lang D., Goodman J., 2013, PASP, 125, 306
- Goldstein H., 1980 Classical Mechanics. Addison-Wesley, Reading, MA
- Hartmann M., Debattista V. P., Seth A., Cappellari M., Quinn T. R., 2011, MNRAS, 418, 2697
- Hilbert D., Cohn-Vossen S., 1999, Geometry and the Imagination. Chelsea Publishing Company, New York
- Ivezić Ž. et al., 2008, ApJ, 684, 287
- Jeans J. H., 1919, Problems of Cosmogony and Stellar Dynamics. Cambridge Univ. Press, Cambridge
- Kepley A. A. et al., 2007, AJ, 134, 1579
- King C., III, Brown W. R., Geller M. J., Kenyon S. J., 2015, ApJ, 813, 89
- Koposov S., Rix H.-W., Hogg D., 2010, 712, 260
- Lablanche P.-Y. et al., 2012, MNRAS, 424, 1495
- Landau L. D., Lifshitz E. M., 1976, Mechanics. Pergamon Press, Oxford
- Levi-Civita T., 1904, Math. Ann., 59, 383
- Loebman S. R. et al., 2014, ApJ, 794, 151
- Lupton R. H., Gunn J. E., 1987, AJ, 93, 1106
- Lynden-Bell D., 1960, PhD thesis, Cambridge University
- Lynden-Bell D., 1962, MNRAS, 124, 95
- Makarov A. A., Smorodinsky J. A., Valiev K., Winternitz P., 1967, Nuovo Cimento A, 52, 1061
- Morse P., Feschbach H., 1953, Methods of Theoretical Physics. McGraw-Hill, New York
- Munn J. A. et al., 2004, AJ, 127, 3034
- Piffl T. et al., 2014, MNRAS, 445, 3133
- Pontzen A., Roškar R., Stinson G., Woods R., 2013, Astrophysics Source Code Library, record ascl:1305.002
- Sanders J. L., Evans N. W., 2015, MNRAS, 454, 299
- Schwarzschild M., 1979, ApJ, 232, 236
- Smith M. C. et al., 2009a, MNRAS, 399, 1223
- Smith M. C., Evans N. W., An J. H., 2009b, ApJ, 698, 1110
- Stäckel P., 1891, Ueber die integration der Hamilton-Jacobischen Differentialgleichung mittelst Separation der Variablen, Habilitationsschrift, Halle
- Syer D., Tremaine S., 1996, MNRAS, 282, 223
- van de Ven G., Hunter C., Verolme E. K., de Zeeuw P. T., 2003, MNRAS, 342, 1056
- van de Ven G., Falcón-Barroso J., McDermid R. M., Cappellari M., Miller B. W., de Zeeuw P. Tim, 2010, ApJ, 719, 1481
- van der Marel R. P., 1994, MNRAS, 270, 271
- Weinacht J., 1924, Math. Ann., 91, 279
- Whittaker E. T., 1917, Analytical Dynamics. Cambridge Univ. Press, Cambridge
- Wilkinson M. I., Evans N. W., 1999, MNRAS, 310, 645
- Williams A. A., Evans N. W., 2015, MNRAS, 454, 698.
- Woolley R., 1978, MNRAS, 184, 311
- Zhao H., 1996, MNRAS, 278, 488

## APPENDIX A: EDDINGTON POTENTIALS WITHOUT TEARS

The separable potentials in spherical polars

$$\psi = \psi_1(r) + \frac{\psi_2(\theta)}{r^2} + \frac{\psi_3(\phi)}{r^2 \sin^2 \theta}, \quad (\text{A1})$$

were introduced into stellar dynamics by Eddington. They are often called Eddington potentials in the astronomical literature (e.g. Clark 1937; Lynden-Bell 1962; Lupton & Gunn 1987). Astrophysically useful potentials must have  $\psi_3(\phi) = 0$  to avoid singularities all along the polar axis.

The density then must have form

$$\rho = \rho_0(r) + \frac{g(\theta)}{r^4}. \quad (\text{A2})$$

This may also seem objectionable as the density has a serious divergence at the origin. In fact, Eddington (1915) himself believed that  $\psi_2(\theta) = 0$  and so  $g(\theta) = 0$  for practical solutions. However, this is not the case, as the awkwardness can be avoided by requiring the non-spherical part of the density to fall like  $r^{-4}$  only outside the central region.

We now give a simple example of an axisymmetric density distribution that has such a property. We choose the density as

$$\rho(r, \theta) = \rho_0(r) + \rho_2(r)P_2(\cos \theta), \quad (\text{A3})$$

where  $P_2$  is the Legendre polynomial. For flattened systems with everywhere positive mass density, we need  $\rho_2 \leq 0$  and  $\rho_0(r) + \rho_2(r) \geq 0$  for all  $r > 0$ . The gravitational potential of such systems is given by

$$\psi = \psi_0(r) + h(r)P_2(\cos \theta), \quad (\text{A4})$$

where

$$\frac{\psi_0(r)}{4\pi G} = \frac{1}{r} \int_0^r r^2 \rho_0(r) dr + \int_r^\infty r \rho_0(r) dr \quad (\text{A5})$$

and

$$\frac{5}{4\pi G} h(r) = \frac{1}{r^3} \int_0^r r^4 \rho_2(r) dr + r^2 \int_r^\infty \rho_2(r) \frac{dr}{r}. \quad (\text{A6})$$

We wish to have  $h \propto r^{-2}$  for  $r \geq r_0$ . In this region, we need to set  $\rho_2(r) = \rho_2(r_0)(r_0/r)^4$  to ensure a continuous density.

We now define  $K$  to be

$$K = \int_0^{r_0} [r^4 \rho_2(r) - r_0^4 \rho_2(r_0)] dr \quad (\text{A7})$$

and we evaluate our formula for  $h$  at  $r > r_0$  to get

$$\frac{h(r)}{4\pi G} = \frac{K}{5r^3} + \frac{r_0^4 \rho_2(r_0)}{4r^2}. \quad (\text{A8})$$

Evidently, the potential is of the desired form for  $r > r_0$  provided that  $\rho_2(r)$  for  $r < r_0$  obeys the simple integral constraint that  $K = 0$ . Only for  $r > r_0$  is the potential of separable form. Orbits whose pericentres satisfy  $r_p > r_0$  lie within rectangular toroids and have three exact integrals of motion.

## APPENDIX B: ALIGNMENT IN ELLIPSOIDAL COORDINATES

Ellipsoidal coordinates  $(\lambda, \mu, \nu)$  are the most natural coordinates to study triaxial stellar systems (e.g. Lynden-Bell 1962; de Zeeuw 1985; van de Ven et al. 2003; Sanders & Evans 2015). The scale factors are

$$\begin{aligned} P^2 &= \frac{(\lambda - \mu)(\lambda - \nu)}{4(\lambda + a)(\lambda + b)(\lambda + c)}, \\ Q^2 &= \frac{(\mu - \lambda)(\mu - \nu)}{4(\mu + a)(\mu + b)(\mu + c)}, \\ R^2 &= \frac{(\nu - \mu)(\nu - \lambda)}{4(\nu + a)(\nu + b)(\nu + c)}, \end{aligned} \quad (\text{B1})$$

where  $a, b$  and  $c$  are constants that define two sets of foci. Surfaces of constant  $\lambda, \mu$  and  $\nu$  are confocal ellipsoids, one-sheeted hyperboloids and two-sheeted hyperboloids, respectively. The coordinate system is illustrated in e.g. Hilbert & Cohn-Vossen (1999), de Zeeuw (1985) or Boccaletti & Pucacco (1996).

We start by assuming that the second velocity moment ellipsoid is diagonalized in confocal ellipsoidal coordinates, so that all the cross-terms  $\langle v_\lambda v_\mu \rangle, \langle v_\lambda v_\nu \rangle$  and  $\langle v_\mu v_\nu \rangle$  all vanish. The Hamiltonian is

$$H = \frac{1}{2} \left( \frac{p_\lambda^2}{P^2} + \frac{p_\mu^2}{Q^2} + \frac{p_\nu^2}{R^2} \right) - \psi(\lambda, \mu, \nu), \quad (\text{B2})$$

where  $p_\lambda = P^2 \dot{\lambda}$ ,  $p_\mu = P^2 \dot{\mu}$  and  $p_\nu = P^2 \dot{\nu}$  are canonical momenta. Again, as the Hamiltonian is time-invariant, we can always construct the even part of the DF and assume that it depends on the squares of the canonical momenta only. For the cross-terms to vanish in ellipsoidal coordinates, this means  $F_e = F_e(p_\lambda^2, p_\mu^2, p_\nu^2, \lambda, \mu, \nu)$ . Using the Hamiltonian to eliminate  $p_\lambda^2$  without loss of generality, we obtain  $F_e(H, p_\mu^2, p_\nu^2, \lambda, \mu, \nu)$ . Taking the Poisson bracket  $\{F_e, H\} = 0$  tells us that  $F_e$  is independent of  $\lambda$  as well as  $p_\lambda$ . We find, after some work

$$A_1 \frac{\partial F_e}{\partial p_\mu} + A_2 \frac{\partial F_e}{\partial p_\nu} = \frac{p_\mu}{Q^2} \frac{\partial F_e}{\partial \mu} + \frac{p_\nu}{R^2} \frac{\partial F_e}{\partial \nu} \quad (\text{B3})$$

with

$$\begin{aligned} A_1 &= \frac{1}{\lambda - \mu} \\ &\times \left[ \frac{p_\mu^2}{2} \frac{\partial}{\partial \mu} \left( \frac{\lambda - \mu}{Q^2} \right) + \frac{p_\nu^2}{2} \frac{\partial}{\partial \mu} \left( \frac{\lambda - \mu}{R^2} \right) - \frac{\partial}{\partial \mu} ((\lambda - \mu)\psi) + H \right] \end{aligned} \quad (\text{B4})$$

and

$$\begin{aligned} A_2 &= \frac{1}{\lambda - \nu} \\ &\times \left[ \frac{p_\mu^2}{2} \frac{\partial}{\partial \nu} \left( \frac{\lambda - \nu}{Q^2} \right) + \frac{p_\nu^2}{2} \frac{\partial}{\partial \nu} \left( \frac{\lambda - \nu}{R^2} \right) - \frac{\partial}{\partial \nu} ((\lambda - \nu)\psi) + H \right]. \end{aligned} \quad (\text{B5})$$

We are at liberty to send  $p_\mu \rightarrow -p_\mu$  or to send  $p_\nu \rightarrow -p_\nu$  as the DF is invariant under such changes. This tells us that the two equations

$$\begin{aligned} A_1 \frac{\partial F_e}{\partial p_\mu} &= \frac{p_\mu}{Q^2} \frac{\partial F_e}{\partial \mu}, \\ A_2 \frac{\partial F_e}{\partial p_\nu} &= \frac{p_\nu}{R^2} \frac{\partial F_e}{\partial \nu}, \end{aligned} \quad (\text{B6})$$

must be separately satisfied. Now, take the first equation, multiply by  $(\lambda - \mu)$  and differentiate with respect to  $\lambda$ . We already know that  $F_e$  is independent of  $\lambda$  and that  $H$  may be treated as a constant, so this operator annihilates all terms bar the one containing the potential and leaves us with

$$\frac{\partial^2}{\partial \lambda \partial \mu} ((\lambda - \mu)\psi) = 0. \quad (\text{B7})$$

Similarly, multiplying the second equation by  $(\lambda - \nu)$  and differentiating with respect to  $\lambda$  leaves us with

$$\frac{\partial^2}{\partial \lambda \partial \nu} ((\lambda - \nu)\psi) = 0. \quad (\text{B8})$$

We could of course have started by eliminating  $p_\mu^2$  in terms of the Hamiltonian, and repeating our steps would yield

$$\frac{\partial^2}{\partial \mu \partial \nu} ((\mu - \nu)\psi) = 0. \quad (\text{B9})$$

This gives us three partial differential equations that the potential must satisfy, and it is straightforward to integrate them up to establish

$$\begin{aligned} \psi(\lambda, \mu, \nu) &= \\ &= \frac{f_1(\lambda)}{(\lambda - \mu)(\lambda - \nu)} + \frac{f_2(\mu)}{(\mu - \lambda)(\mu - \nu)} + \frac{f_3(\nu)}{(\nu - \lambda)(\nu - \mu)}, \end{aligned} \quad (\text{B10})$$

where  $f_1(\lambda), f_2(\mu)$  and  $f_3(\nu)$  are arbitrary functions of the indicated arguments. This is the separable or Stäckel potential in confocal ellipsoidal coordinates.

## APPENDIX C: THE STÄCKEL CONDITION

Rather than demonstrating the theorem for each alignment separately, a more mathematical – but abstract – approach is to derive all possible coordinate systems and gravitational potentials together. This is similar in spirit to the original investigations of Stäckel (1891) and Eddington (1915).

Here, we prove the following theorem (see also An & Evans 2016): suppose that (i) the second velocity moment tensor of a stellar system is aligned in an orthogonal curvilinear coordinate system and has (in general) three unequal axes and that (ii) the stellar system is in a steady state, so that the even part of the DF satisfies the collisionless Boltzmann equation and (iii) the DF is invariant under reversal of the sign of each velocity component. Then, it necessarily follows that the coordinate system is the confocal ellipsoidal coordinates (or one of its limiting cases) and that the gravitational potential is of separable or Stäckel form.

Consider a system with 3 degrees of freedom governed by the Hamiltonian of the form of

$$H = \frac{1}{2} \sum_{k=1}^3 \frac{p_k^2}{h_k^2(q_1, q_2, q_3)} - \psi(q_1, q_2, q_3), \quad (\text{C1})$$

where  $(q_1, q_2, q_3)$  are orthogonal curvilinear coordinates,  $(p_1, p_2, p_3)$  are the corresponding canonical momenta and  $h_1, h_2, h_3$  are the scale factors. Suppose that the system admits an integral of motion of the form,  $F_e = F_e(p_1^2, p_2^2, p_3^2; q_1, q_2, q_3)$  which is recognized as the even part of the DF. The vanishing of the Poisson bracket requires

$$\begin{aligned} \dot{F}_e &= \{F_e, H\} = \sum_i \left( \frac{\partial F_e}{\partial q_i} \frac{\partial H}{\partial p_i} - \frac{\partial H}{\partial q_i} \frac{\partial F_e}{\partial p_i} \right) \\ &= \sum_i p_i \left( \frac{1}{h_i^2} \frac{\partial F_e}{\partial q_i} - 2 \frac{\partial H}{\partial q_i} \frac{\partial F_e}{\partial (p_i^2)} \right) = 0. \end{aligned} \quad (\text{C2})$$

However, both  $H$  and  $F_e$  are invariant under  $p_j \rightarrow -p_j$  for any  $j$ 's, and so it follows that, for  $\forall i \in \{1, 2, 3\}$ ,

$$\frac{\partial F_e}{\partial q_i} = \zeta_i \frac{\partial H}{\partial q_i}, \quad \zeta_i \equiv 2h_i^2 \frac{\partial F_e}{\partial (p_i^2)}. \quad (\text{C3})$$

Here note that, for any  $i$  and  $j$ ,

$$\begin{aligned} \frac{\partial \zeta_i}{\partial q_j} &= 2h_i^2 \frac{\partial^2 F_e}{\partial q_j \partial (p_i^2)} + 2 \frac{\partial h_i^2}{\partial q_j} \frac{\partial F_e}{\partial (p_i^2)} \\ &= 2h_i^2 \frac{\partial}{\partial (p_i^2)} \left( \zeta_j \frac{\partial H}{\partial q_j} \right) + \frac{\zeta_i}{h_i^2} \frac{\partial h_i^2}{\partial q_j} \\ &= 2h_i^2 \frac{\partial \zeta_j}{\partial (p_i^2)} \frac{\partial H}{\partial q_j} + 2h_i^2 \zeta_j \frac{\partial^2 H}{\partial (p_i^2) \partial q_j} + \frac{\zeta_i}{h_i^2} \frac{\partial h_i^2}{\partial q_j} \\ &= 4h_i^2 h_j^2 \frac{\partial^2 F_e}{\partial (p_i^2) \partial (p_j^2)} \frac{\partial H}{\partial q_j} + h_i^2 \zeta_j \frac{\partial}{\partial q_j} \left( \frac{1}{h_i^2} \right) + \frac{\zeta_i}{h_i^2} \frac{\partial h_i^2}{\partial q_j} \\ &= 4h_i^2 h_j^2 \frac{\partial^2 F_e}{\partial (p_i^2) \partial (p_j^2)} \frac{\partial H}{\partial q_j} + \frac{\zeta_i - \zeta_j}{h_i^2} \frac{\partial h_i^2}{\partial q_j}. \end{aligned} \quad (\text{C4})$$

Then the integrability condition on  $F_e$  is

$$\frac{\partial}{\partial q_i} \left( \frac{\partial F_e}{\partial q_j} \right) - \frac{\partial}{\partial q_j} \left( \frac{\partial F_e}{\partial q_i} \right) = 0 \quad (\text{C5})$$

which results in

$$\begin{aligned} &\frac{\partial}{\partial q_i} \left( \zeta_j \frac{\partial H}{\partial q_j} \right) - \frac{\partial}{\partial q_j} \left( \zeta_i \frac{\partial H}{\partial q_i} \right) \\ &= \frac{\partial \zeta_j}{\partial q_i} \frac{\partial H}{\partial q_j} - \frac{\partial \zeta_i}{\partial q_j} \frac{\partial H}{\partial q_i} + \zeta_j \frac{\partial^2 H}{\partial q_i \partial q_j} - \zeta_i \frac{\partial^2 H}{\partial q_j \partial q_i} \\ &= \frac{\zeta_j - \zeta_i}{h_j^2} \frac{\partial h_j^2}{\partial q_i} \frac{\partial H}{\partial q_j} - \frac{\zeta_i - \zeta_j}{h_i^2} \frac{\partial h_i^2}{\partial q_j} \frac{\partial H}{\partial q_i} + (\zeta_j - \zeta_i) \frac{\partial^2 H}{\partial q_i \partial q_j} \\ &= (\zeta_j - \zeta_i) \mathcal{D}_{ij}(H) = 0 \quad (\text{for all } i, j). \end{aligned} \quad (\text{C6})$$

Here,  $\mathcal{D}_{ij}(f)$  is the linear second-order differential operator acting on a function  $f(q_1, q_2, q_3)$ , defined as

$$\begin{aligned} \mathcal{D}_{ij}(f) &\equiv \frac{1}{h_j^2} \frac{\partial h_j^2}{\partial q_i} \frac{\partial f}{\partial q_j} + \frac{1}{h_i^2} \frac{\partial h_i^2}{\partial q_j} \frac{\partial f}{\partial q_i} + \frac{\partial^2 f}{\partial q_i \partial q_j} \\ &= \left( \frac{\partial \ln h_j^2}{\partial q_i} \frac{\partial}{\partial q_j} + \frac{\partial \ln h_i^2}{\partial q_j} \frac{\partial}{\partial q_i} + \frac{\partial^2}{\partial q_i \partial q_j} \right) f, \end{aligned} \quad (\text{C7})$$

which is symmetric for  $i \leftrightarrow j$ , i.e.  $\mathcal{D}_{ij}(f) = \mathcal{D}_{ji}(f)$ . In other words, if there exists an integral  $F_e$ , we must have  $\zeta_i = \zeta_j$  or  $\mathcal{D}_{ij}(H) = 0$  for any pair of indices  $i$  and  $j$ . The  $\zeta_i = \zeta_j$  (for  $i \neq j$ ) case however implies that the integral  $F_e$  becomes invariant under the rotation within  $p_i$ - $p_j$  plane and so the distribution must be isotropic within  $q_i$ - $q_j$  plane: that is to say, the resulting second velocity moments must be degenerate as in  $\langle v_i^2 \rangle = \langle v_j^2 \rangle$ . If  $\zeta_i \neq \zeta_j$  on the other hand, we must have

$$\begin{aligned} \mathcal{D}_{ij}(H) &= \frac{1}{2} \sum_k \mathcal{D}_{ij} \left( \frac{1}{h_k^2} \right) p_k^2 - \mathcal{D}_{ij}(\psi) = 0 \\ \Rightarrow \mathcal{D}_{ij}(h_k^{-2}) &= \mathcal{D}_{ij}(\psi) = 0. \end{aligned} \quad (\text{C8})$$

The condition on the scale factors  $\mathcal{D}_{ij}(h_k^{-2}) = 0$  for all  $i \neq j$  (and any  $k$ ) is the same condition defining the Stäckel systems. The most general orthogonal curvilinear coordinate in a Euclidean space that satisfies the condition is the confocal ellipsoidal coordinates. This encompasses the 11 3D quadric coordinates in which the Helmholtz equation separates (Morse & Feshbach 1953). On the other hand, the general solution of  $\mathcal{D}_{ij}(\psi) = 0$  in the confocal ellipsoidal coordinates (or its degenerate limit) is known to be  $\psi(q_1, q_2, q_3) = \sum_k f_k(q_k)/h_k^2$  where  $f_k(q_k)$  is an arbitrary function of the coordinate component  $q_k$  alone.

The condition  $\mathcal{D}_{ij}(\psi) = 0$  is really the integrability condition on the system of the quasi-linear partial differential equations. If we suppose the existence of the set of functions  $\{f_1(q_1), f_2(q_2), f_3(q_3)\}$  such that  $\psi(q_1, q_2, q_3) = \sum_k f_k(q_k)/h_k^2$ , then

$$\begin{aligned} \frac{\partial \psi}{\partial q_i} &= \frac{f_i'(q_i)}{h_i^2} - \sum_k \frac{\partial h_k^{-2}}{\partial q_i} f_k(q_k) \\ \Rightarrow \frac{\partial f_i}{\partial q_j} &= \delta_i^j h_i^2 \left( \frac{\partial \psi}{\partial q_i} + \sum_k \frac{\partial h_k^{-2}}{\partial q_i} f_k \right), \end{aligned}$$

where  $\delta_i^j$  is the Kronecker delta. This is the system of partial differential equations on  $\{f_1(q_1), f_2(q_2), f_3(q_3)\}$ , whose compatibility condition implies that  $(\partial/\partial q_j)(\partial f_i/\partial q_k) = (\partial/\partial q_k)(\partial f_i/\partial q_j)$  for any  $i, j, k$ . The only non-trivial conditions among these are

$$\begin{aligned} \frac{\partial}{\partial q_j} \left( \frac{\partial f_i}{\partial q_i} \right) &= h_i^2 \left[ \mathcal{D}_{ij}(\psi) - \sum_k \mathcal{D}_{ij}(h_k^{-2}) f_k \right] \\ &= 0 \quad (\text{for any } i \neq j), \end{aligned}$$

and so, given the Stäckel coordinate satisfying  $\mathcal{D}_{ij}(h_k^{-2}) = 0$ , we find that  $\mathcal{D}_{ij}(\psi) = 0$  is the necessary condition for existence of the solution set  $\{f_1, f_2, f_3\}$ . Moreover, thanks to the Frobenius theorem, the condition is also sufficient for (local) existence of such a solution set. In other words,  $\psi(q_1, q_2, q_3) = \sum_k f_k(q_k)/h_k^2$  is also in fact the general solution of  $\mathcal{D}_{ij}(\psi) = 0$ .

A consequence of this theorem is that it seems to imply that the only axisymmetric equilibria with DFs are either (i) Jeans models with  $F = F(E, L_z)$  in which two of the semi-axes of the second moment tensor are the same or (ii) Stäckel or separable models in spheroidal coordinates with all three semi-axes different. This seems to cast doubt on the existence of axisymmetric equilibria constructed by Schwarzschild modelling (see e.g. Cretton et al. 1999). However, the likely resolution of this paradox is that the only regular orbits observing the required symmetry are those in separable potentials, and so the velocity distributions resulting from a Schwarzschild model in a non-separable potential are not strictly symmetric.

This paper has been typeset from a  $\text{\TeX}/\text{\LaTeX}$  file prepared by the author.